

CloudSat Project

A NASA Earth System Science Pathfinder Mission

CloudSat 2B-CLDCLASS-LIDAR Product Process Description and Interface Control Document

Product Version: P1_R05

Document Revision: 0

Date: 10 April 2019

Questions concerning the document and proposed changes shall be addressed to

Zhien Wang
Zhien.Wang@colorado.edu
303-492-1613

Document Revision History

Date	Revision	Description	Section(s) Affected
April 2019	0	Initial Release	All

Table of Contents

1	Introduction	4
2	Algorithm Theoretical Basis	7
3	Algorithm Inputs	13
3.1	CloudSat.....	13
3.1.1	Cloud properties from 2B-GEOPROF and 2B-GEOPROF-lidar products	13
3.2	Ancillary (Non-CloudSat)	14
3.2.1	CALIOP.....	14
3.2.2	MODIS	14
3.2.3	ECMWF.....	14
3.2.4	Coastline Map	14
3.2.5	Topographical Map	15
3.3	Input Variable Summary.....	15
3.4	Control and Calibration	15
4	Algorithm Summary	16
4.1	Cloud clustering analysis	16
4.2	The flowchart of cloud scenario classification	18
4.3	Classification Method	19
4.4	Precipitation Identification	25
4.5	Cloud Phase Identification.....	25
5	Data Product Output Format	30
6	Operator Instructions.....	30
7	References	35
8	Acronym List.....	37
9	Changes Since Algorithm Version P_R04	37
10	Open Issues and comments	38
11	Appendix A: 2B-CLDCLASS-LIDAR Interface Control Document	39
11.1	Input Field Specifications	39
11.2	Product Field Specifications.....	49

1 Introduction

A great strength of microwave radar measurements of clouds and precipitation is the ability to retrieve quantitative content data from the radar reflectivity factor Z . This is made possible by devising algorithms based on empirical relationships between Z and various microphysical parameters, such as ice water content IWC or rainfall rate. However, because of the diversity of microphysical conditions found in the atmosphere, algorithms need to be applied only to those conditions for which they are considered valid. In other words, it is first necessary to identify the target and then select an appropriate algorithm. This is true to implement sophisticated multi-sensor retrieval algorithms. The algorithm selection process depends on such basic factors as cloud phase, and also the hydrometeor density, shape, and size distribution. For example, although cirrus, altostratus, and the upper portions of cumulonimbus clouds are all predominantly ice phase clouds, it is not possible to apply a single algorithm for retrieving IWC in these targets: cirrus generally contain only single ice crystals, altostratus likely contain low-density ice crystal aggregates at the warmer temperatures, and cumulonimbus may combine ice crystals, snowflakes, rimed particles, graupel, and even hailstones. Due to the different radiative forcings of various cloud types (Hartmann et al. 1992; Chen et al. 2000), classifying clouds into categories based on type is also an important task for cloud remote sensing and global cloud climatology studies.

As the first step in converting the vertical profiles of Z from CloudSat into meaningful microphysical data quantities, we are developing an algorithm for identifying cloud type and precipitation. However, measurements of cloud radar alone cannot provide necessary information for cloud scenario classification. The formation fly (A-train) of Aqua, CloudSat and CALIPSO provides other cloud information from lidar and passive radiometer measurements. As described here, we identify eight basic cloud types that are recognized by surface observers internationally by combining information available mainly from the CloudSat and CALIPSO satellites.

a) Different detection sensitivities of lidar and cloud radar

The main difference between lidar and cloud radar is their working wavelengths: optical wavelength for lidar and millimeter wavelength for cloud radar. Table 1 provides the specifications of CloudSat Cloud Profiling Radar (CPR) and CALIPSO lidar (CALIOP). The different wavelengths result in different sensitivities of lidar and radar for cloud particles. Lidar is sensitive enough to detect clouds and aerosols in the troposphere, but its short wavelength results in strong attenuation from them and limits its ability to penetrate optically thick clouds to detect anything beyond them. Lidar, especially space based, is more suitable to profile high and mid-level clouds due to their lower optical thicknesses than low-level clouds. Cloud detection with millimeter cloud radar (k-band

and w-band) has some distinct advantages compared to lidar. For example, 8-mm and 3-mm cloud radars can penetrate optically thick clouds to detect multi-layer cloud systems. However, its long wavelength limits its capability to detect midlevel supercooled water clouds with relatively small water droplets or cold ice clouds with low concentrations of small ice crystals. However, for mixed phase clouds or water clouds with drizzle, cloud radar signals are dominated by the backscatter of ice particles or drizzle-size drops.

Table 1: The specifications of CPR and CALIOP

	CALIOP	CPR
λ	0.532/1.06 μm	3200 μm
Pulse Width	~ 10 ns	3.3/33.3 μsec
PRF	~ 20 Hz	4300/800Hz
$P_t(\lambda)$	10^5 - 10^6 W (peak)	~ 270 W (avg)
Scatter of Cloud particles	Mie scatter	Rayleigh/Mie scatter
Backscattering of cloud particles	$\propto D^2$	$\propto D^6 / \propto D^2$
Attenuation of Clouds	Strong	Weak

Their different sensitivities are illustrated with following examples. Figure 1 presents examples from ground-based lidar and radar Measurements. The left side of Fig. 1 is a midlatitude case, and shows that cloud radar (top) misses to detect supercooled water clouds, which are optically thick enough to attenuate lidar to detect high cirrus clouds. Another interesting point is that cloud radar detects strong signal from virga because it is much sensitive to larger particles than lidar. The right side of Fig. 1 presents a case from the Arctic, and different cloud images are seen from lidar and radar measurements for

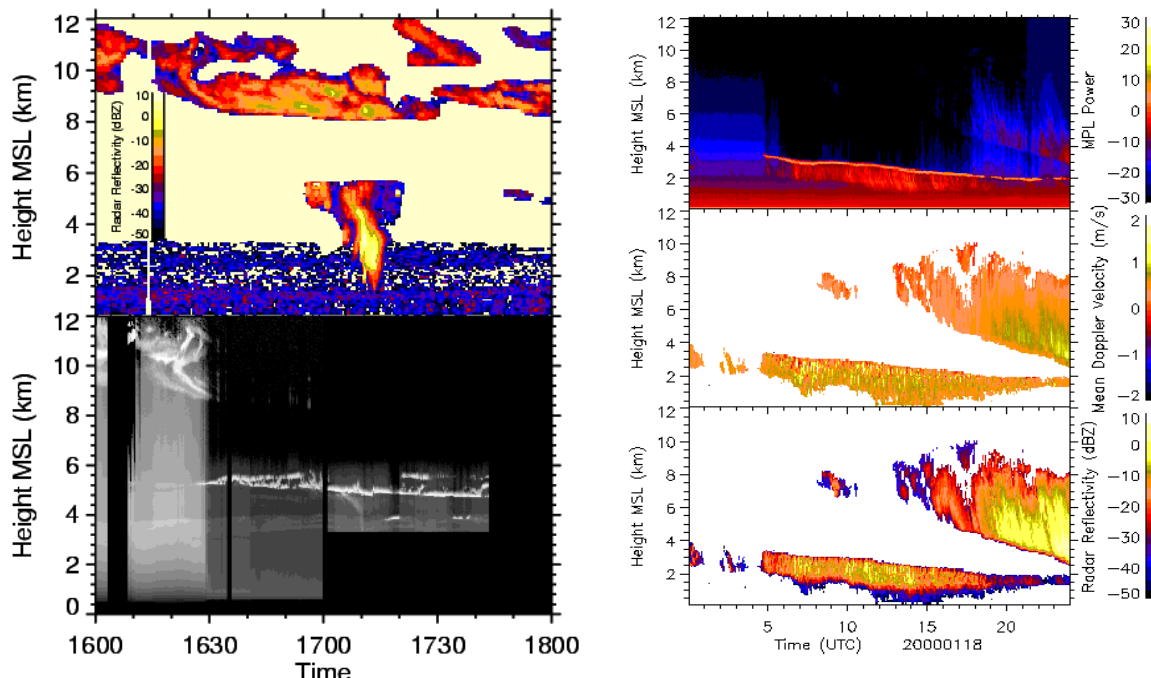


Figure 1. Co-located ground-based lidar and radar measurements. Left: Cloud radar Ze (top) and lidar return (bottom) for middle-level and high cloud layers observed at the SGP site. Right: the time-height display of lidar return (top), mean Doppler velocity (middle) and Ze profiles (bottom) for mixed-phase and ice cloud layers observed at the NSA site

precipitating altocumulus clouds. Lidar measurements show strong signals for supercooled water-dominated source clouds whereas radar measurements show strong signals for ice virga because of their different sensitivities to cloud particle sizes.

Figure 2 show a collocated CloudSat CALIPSO example. It is clear that lidar can detect optically thin cirrus clouds in the tropics that are missed by the radar, and lidar signals are strongly attenuated by the optically thick clouds. On the other hand, radar shows better capabilities to profile optically thick clouds and moderate precipitation. But radar has some difficulties to detect stratocumulus without drizzle.

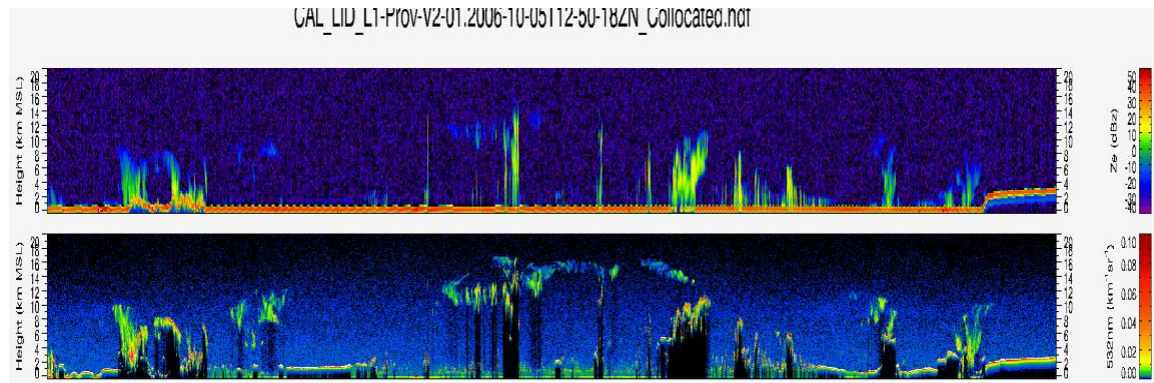


Figure 2. Collocated CloudSat (top) and CALIPSO lidar (532 nm) lidar measurements over a half nighttime orbit on 5 October 2006.

b) Different vertical and horizontal resolutions of CPR and CALIOP

The CPR and CALIOP profile cloud 2-D structure at different horizontal and vertical resolutions as given in Table 2. For clouds below 8.2 km, a CPR footprint contains ~ 12 CALIOP footprints, thus CALIOP measurements are able to provide fine cloud structure within a CPR footprint. This fine structure is important to characterize cumulus and stratocumulus clouds. The CALIOP also has better vertical resolution than that of CPR, which is important for geometrically thin cloud layer detection, such as altocumulus.

Table 2: The horizontal and vertical resolutions of CPR and CALIOP

Altitude Region (km)	Horizontal (km)			Vertical (meters)	
	CPR	CALIOP	CPR	CALIOP	CALIOP
-2.0 to -0.5		1/3		300	
-0.5 to 8.2	1.4x1.8	1/3	500/240	30	
8.2 to 20.2	1.4x1.8	1	500/240	60	

20.2 to 25.0	1.4x1.8	5/3	500/240	180
25.0 to 30.1		5/3		180
30.1 to 40.0		5		300

In summary, combining lidar and radar measurements provide better cloud detection and characterization because of their unique complementary capabilities. Now combining radar and lidar measurements are widely used for cloud studies from cloud macrophysical and microphysical properties. CloudSat and CALIPSO satellites will provide us first opportunity to study cloud from space by combining lidar and radar measurements. In general, cloud optical thickness decreases with altitude (as temperature decrease), thus lidar has more chances to penetrate high and midlevel clouds than low-level clouds. Therefore, there are more advantages to combine lidar and radar measurements from space than from ground. In this document, we discuss how to combine CPR and CALIOP measurements for the cloud phase determination and cloud scenario classification. Combining CPR and CALIOP measurements for ice cloud microphysical property retrievals is provided by the 2C-ICE product (Deng et al. 2010).

2 Algorithm Theoretical Basis

Algorithms based on different cloud spectral, textural, and physical features have been developed for cloud classification from satellites (Welch et al. 1992; Tovinkere et al. 1993; Bankert 1994; Luo et al. 1995; Rossow and Schiffer 1999). The International Satellite Cloud Climatology Project (ISCCP) (Rossow and Schiffer 1999) uses the combination of cloud top pressure and cloud optical depth to classify clouds into either cumulus (Cu), stratocumulus (Sc), stratus (St), altocumulus (Ac), altostratus (As), nimbostratus (Ns), cirrus, cirrostratus, or deep convective clouds. Table 3 shows the basic features of these different cloud types (WMO 1956; Parker 1988; Uddstrom and Gray 1996; Moran et al. 1997). However, with more long-term ground-based remote sensing cloud studies underway, algorithms to classify cloud type using ground-based measurements were developed. Wang and Sassen (2001) developed an algorithm to classify clouds by combining the measurements of ground-based multiple remote sensors. Duchon and O'Malley (1999) studied the possibility of classifying clouds according to ground-based solar flux measurements. Williams et al. (1995) developed an algorithm to classify precipitating clouds into either stratiform, mixed stratiform, convective, and deep or shallow convective clouds using 915-MHz wind profile data.

In this document, we present a new algorithm for CloudSat to classify clouds into either St, Sc, Cu, Nb, Ac, As, deep convective, or high cloud by combining space-based active (CPR and CALIOP) and passive remote sensing (MODIS) data. The class of high cloud includes cirrus, cirrocumulus, and cirrostratus, and Cu cloud represents cumulus congestus and fair weather cumulus. These types may be further classified into sub-types to refine IWC and LWC retrievals.

Table 3 Characteristic cloud features for the major cloud types derived from numerous studies (midlatitude). Our cloud type identification algorithm is based on many of these characteristics. Heights are above ground level.

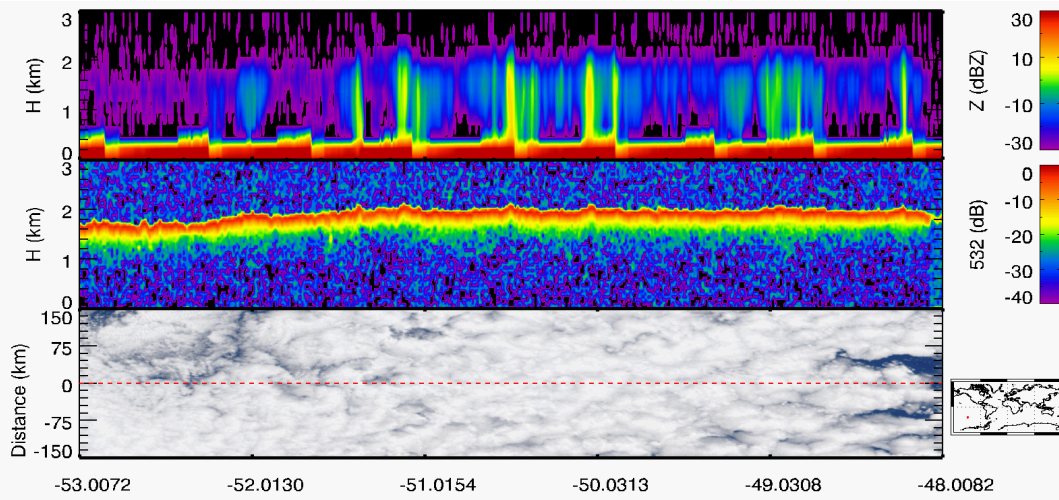
Cloud Class	Cloud Features	
High Cloud	Base	> 7.0 km
	Rain	no
	Horiz. Dim.	1 to 10 ³ km
	Vert. Dim.	moderate
	LWP	= 0.
As	Base	2.0-7.0 km
	Rain	none
	Horiz. Dim.	10 ³ km, homogeneous
	Vert. Dim.	moderate
	LWP	~ 0, dominated by ice
Ac	Base	2.0-7.0 km
	Rain	virga possible
	Horiz. Dim.	10 ³ km, inhomogeneous
	Vert. Dim.	shallow or moderate
	LWP	> 0
St	Base	0-2.0 km
	Rain	none or slight
	Horiz. Dim.	10 ² km, homogeneous
	Vert. Dim.	shallow
	LWP	> 0.
Sc	Base	0.-2.0 km
	Rain	drizzle or snow possible
	Horiz. Dim.	10 ³ km, inhomogeneous
	Vert. Dim.	shallow
	LWP	> 0.
Cu	Base	0-3.0 km
	Rain	drizzle or snow possible
	Horiz. Dim.	1 km or larger, isolated
	Vert. Dim.	shallow or moderate
	LWP	> 0.
Nb	Base	0-4.0 km
	Rain	prolonged rain or snow
	Horiz. Dim.	50 -1000 km
	Vert. Dim.	thick

	LWP	> 0.
Deep convective clouds	Base	0-3.0 km
	Rain	intense shower of rain or hail possible
	Horiz. Dim.	10 km or large
	Vert. Dim.	thick
	LWP	> 0.

a) Measurements used for cloud classification

We classify clouds by using vertical and horizontal cloud properties, the presence or absence of precipitation, cloud temperature, and upward radiance from MODIS measurements. The CPR and CALIOP provide vertical cloud profiles and horizontal extent of clouds, which provide important information to differentiate cloud types. Figure 3 displays CloudSat CPR and CALIPSO CALIOP measurements for close and open cell stratocumulus, which clearly show different sensitivities of lidar and radar for cloud and precipitation measurements. This figure also shows horizontal and vertical variability for different types of clouds.

a)



b)

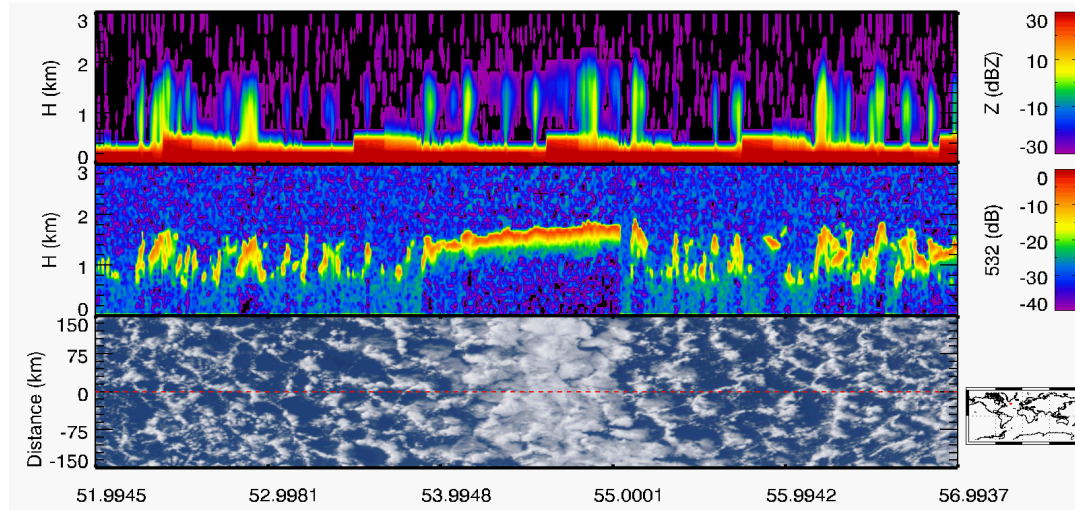


Figure 3: Examples of ‘3-D’ cloud measurements from the A-train satellites: a) close cell stratocumulus and b) open and clous cell stratocumulus. For each example, from top to bottom are CloudSat Z_e , CALIPSO lidar attenuated backscattering, and MODIS true color image.

In addition to active remote sensing data, MODIS radiance measurements from Aqua satellite can be incorporated into the algorithm. Cloud spectral, and textural features derived from radiance data are important supplementary information to cloud vertical and horizontal extents from active remote sensors. However, these MODIS measurements are mainly useful for single layer cloud system. Combing active and passive remote sensing from space provides kind of three-dimensional cloud structure as showed in the Fig. 3.

The CALIOP also provides lidar linear depolarization ratios (δ) of clouds, which can be used for cloud phase discrimination in principle (Sassen 1991). However, the strong influence of multi-scattering on δ for space-based lidar measurements limits the potential of using δ directly. Combining δ , attenuated backscattering coefficient and Z_e profiles provide better cloud phase discrimination. Section 4.5 will provide more details on the cloud phase identification by combining CloudSat and CALIPSO measurements.

Table 4 lists important 2-D cloud structures and properties contributed by CPR and CALIOP measurements for different cloud types. It is clear that combined CPR and CALIOP measurements provide improved cloud macrophysical properties.

Table 4: Contributions of CPR and CALIOP measurements on cloud 2-D Structure for different cloud types.

	CPR	CALIOP
High clouds	Boundaries	Fine Boundaries
Altostratus	Boundaries, Max Z_e	Phase, Upper boundary
Alto cumulus	----	Phase, Boundaries
Alto cumulus + virga	Boundaries, Max Z_e	Phase, Boundaries
Cumulus	Boundaries, Max Z_e	Fine horizontal structure
Stratus and stratocumulus	Boundaries, Max Z_e	Phase, Upper boundary
Nimbostratus	Boundaries, Max Z_e	Upper boundary
Deep Convective	Boundaries, Max Z_e	Upper boundary
Multi-layer cloud system	Boundaries, Max Z_e for each layer	Phase and boundaries of upper layer/layers

Cloud temperature (T) derived from ECMWF predictions is an important cloud property. Using our ground-based cloud classification results (Wang and Sassen 2001), we derive the frequency distribution of different cloud types in maximum Z_e and T (at maximum Z_e height) space (see Fig. 4a and 4b). The features displayed in Fig. 4 are consistent with cloud physics and the microphysical properties of different cloud types.

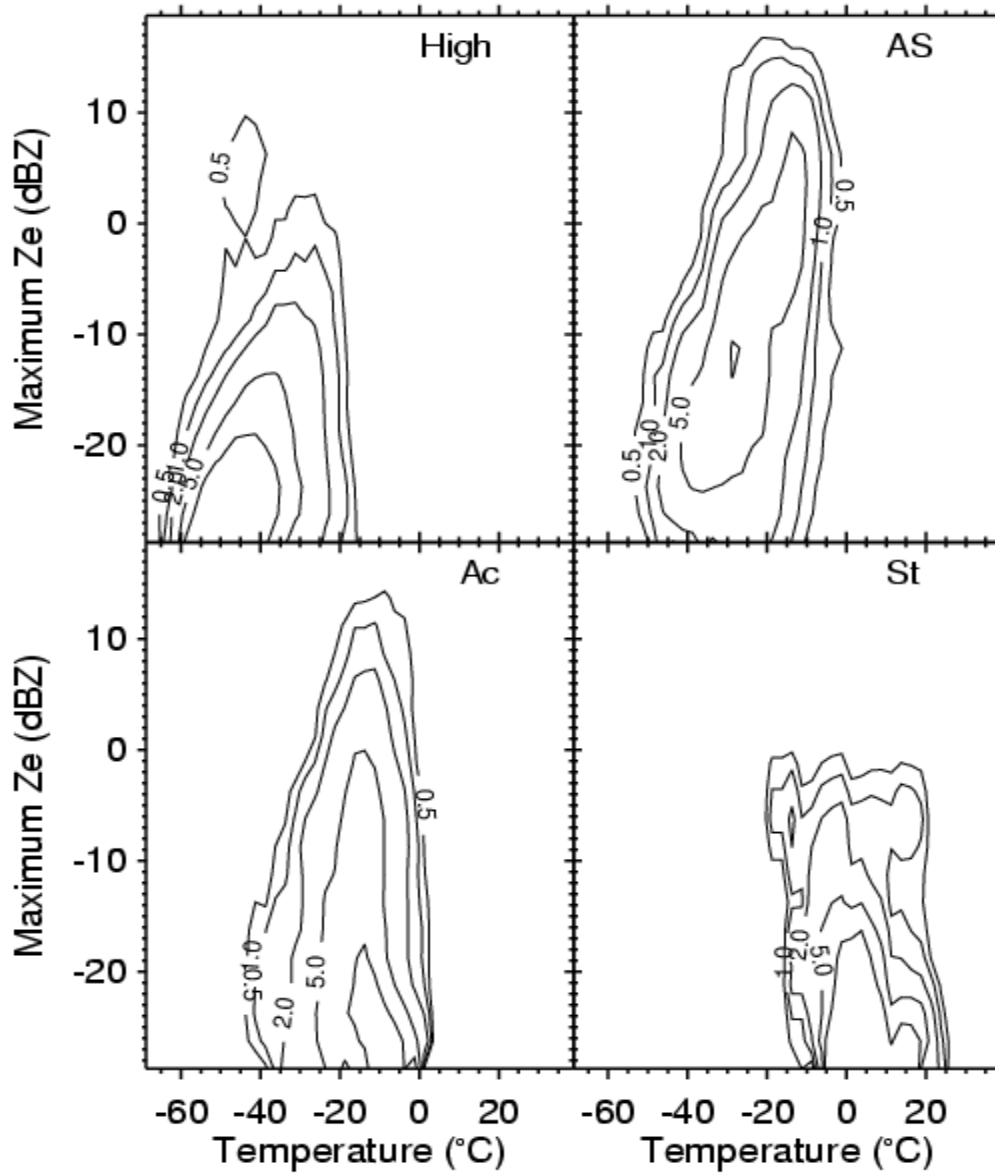


Figure 4a: Frequency distribution of different types of clouds in the temperature and maximum Z_e space.

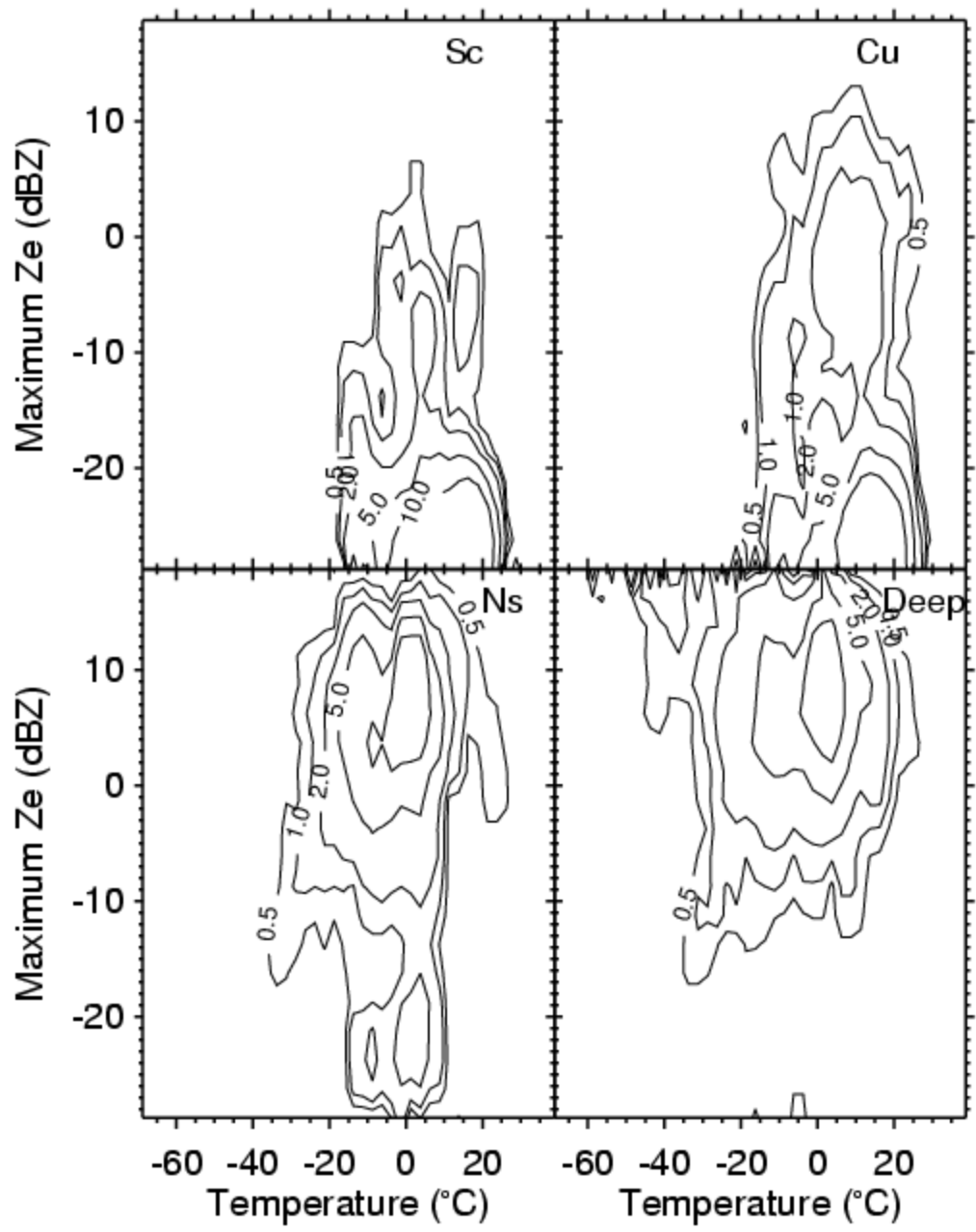


Figure 4b: Frequency distribution of different types of clouds in the temperature and maximum Z_e space.

b) Methodology

Role-based classification methods, which assigns different threshold values to characteristic parameters, are simple and easy to use methods, but the results are sensitive to the selection of the thresholds. Instead of using Boolean logic, the proper use of fuzzy logic can improve the results of cloud classification (Penoloza and Welch 1996). The approach of using neural networks to classify cloud type in satellite imagery has shown recent success (Welch et al. 1992; Bankert 1994). The network is trained on selected spectral, textural, and physical features associated with expertly labeled samples. The trained network is subsequently applied to unknown cloud samples. However, these new classification techniques can not guarantee better performance, which depends on how properly designed the classifier is and the selection of features (Tovinkere et al. 1993).

Combined rule-based and fuzzy logic classification approach is used in this algorithm. We use the following strategy to classify clouds. First, combined radar and lidar cloud mask results are used to find a cloud cluster according to their persistence in the horizontal and vertical directions. A minimum horizontal extent for a cluster is required, therefore, a cloud cluster permits horizontally broken, but vertically similar cloud fields.

Once a cloud cluster is found, cloud height, temperature, and maximum Z_e , as well as the occurrence of precipitation, are determined. Then the cluster mean properties as well as spatial inhomogenities in terms of cloud top height, lidar and radar maximum signals are sent to a fuzzy classifier to classify the cluster into one cloud type with an assigned confidence level.

3 Algorithm Inputs

3.1 *CloudSat*

3.1.1 **Cloud properties from 2B-GEOPROF and 2B-GEOPROF-lidar products**

CPR- Z_e profiles and combined lidar and radar boundaries provide horizontal and vertical cloud structure and are main inputs for cloud scenario classification. Inputs from these two products are: Z_e profile, radar cloud mask, geolocation, altitude of each radar bin, surface bin number, and cloud layer information.

3.2 Ancillary (Non-CloudSat)

3.2.1 CALIOP

3.2.1.1 Lidar level 1 attenuated backscattering coefficients

In the Lidar-AUX product, CALIOP attenuated backscattering coefficients at different horizontal resolutions are averaged to the CloudSat horizontal resolution. But it keeps the data at the native CALIOP vertical resolutions for better cloud boundary and phase identifications.

3.2.1.2 Lidar cloud mask at the CloudSat horizontal resolution

This is provided by the Lidar-AUX product, which identifies clouds based on lidar attenuated backscattering coefficients at CloudSat horizontal and CALIPSO vertical resolutions. Cloud fractions within CloudSat footprints are also provided in this product by using fine horizontally resolved CALIPSO measurements.

3.2.2 MODIS

MODIS radiance data of channel 1, 2, 26, 29, 31, and 32 (Ackerman et al. 1998) could be used as supplementary information to CloudSat radar and CALIPSO lidar measurements for cloud scenario classification. Cloud variability orthogonal to the radar ground track will be explored with MODIS radiance data to improve cumulus-type cloud identification. But at this point, MODIS radiance data are not used in the algorithm due to the unavailability of MODIS data after CloudSat and CALIPSO leaving the A-train.

Table 5: The MODIS bands used in the MODIS cloud mask algorithm

Band	Wavelength (μm)	
1 (250 m)	0.659	Clouds, shadow
2 (250 m)	0.865	low clouds
26	1.375	thin cirrus
29	8.550	cloud
31	11.030	cloud
32	12.020	cloud

3.2.3 ECMWF

Temperature profiles are used.

3.2.4 Coastline Map

Land or ocean flag is used.

3.2.5 Topographical Map

It provides surface altitudes above the sea level to estimate the heights of cloud above the surface.

3.3 Input Variable Summary

See the 2B-CLDCLASS-LIDAR Interface Control Document in the appendix A.

3.4 Control and Calibration

No control and calibration are necessary for this algorithm.

4 Algorithm Summary

First algorithm performs clustering analysis to group individual cloud profiles in to a cluster, then calculate cluster features to classify it as one of the standard cloud type. Figure 5 presents the general block structure of the classification algorithm.

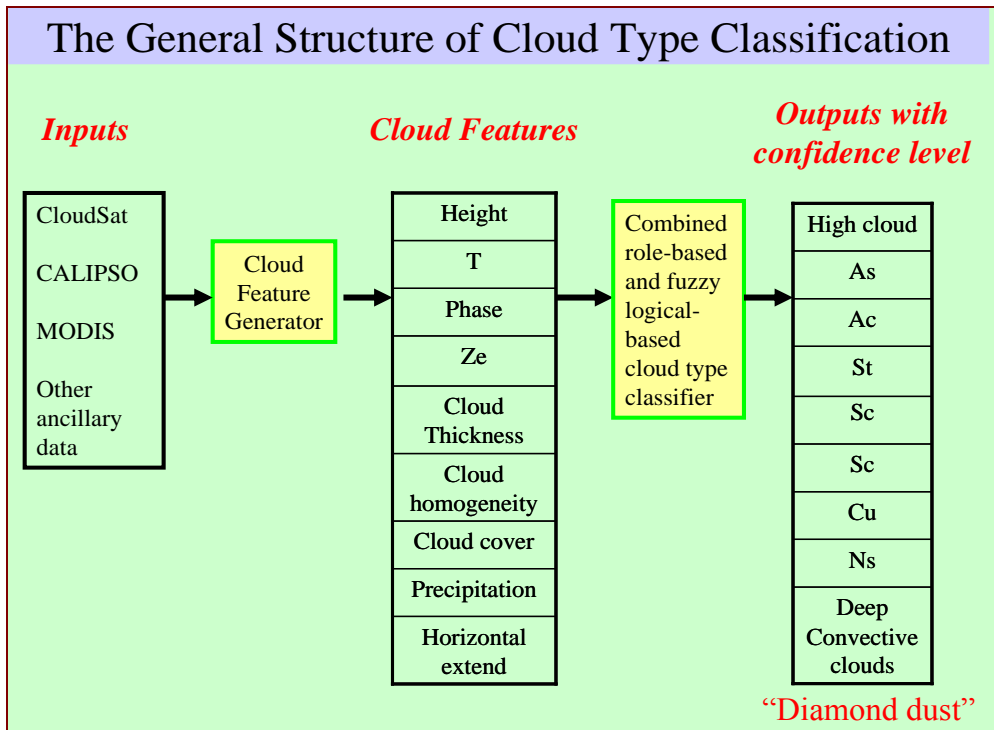


Figure 5. The general function blocks of the classification algorithm.

4.1 Cloud clustering analysis

Cloud Cluster: One or multiple similar cloud elements

Cloud Element: A group of radar and/or lidar detected and horizontally connected cloud cloud layers with a similar vertical extend. Systemaic changes in cloud base or top height, cloud thickness, precipitation, or phase are used to separate horizontally connected cloud layers into different elements.

Because of the strong variabilities of clouds, it is difficult to apply a classification algorithm directly to an individual radar profile. Different types of clouds have different horizontal and vertical extents. The cloud clustering analysis provides cloud horizontal and vertical extent features. For some cloud types, such as Cu and Sc, horizontal extent of a cloud element may be small. Therefore, it is necessary to allow breaks between cloud elements to group multiple similar cloud elements together for the classification. A

CloudSat granule may be divided into a different number of cloud clusters varying with cloud types presented in the granule.

4.2 The flowchart of cloud scenario classification

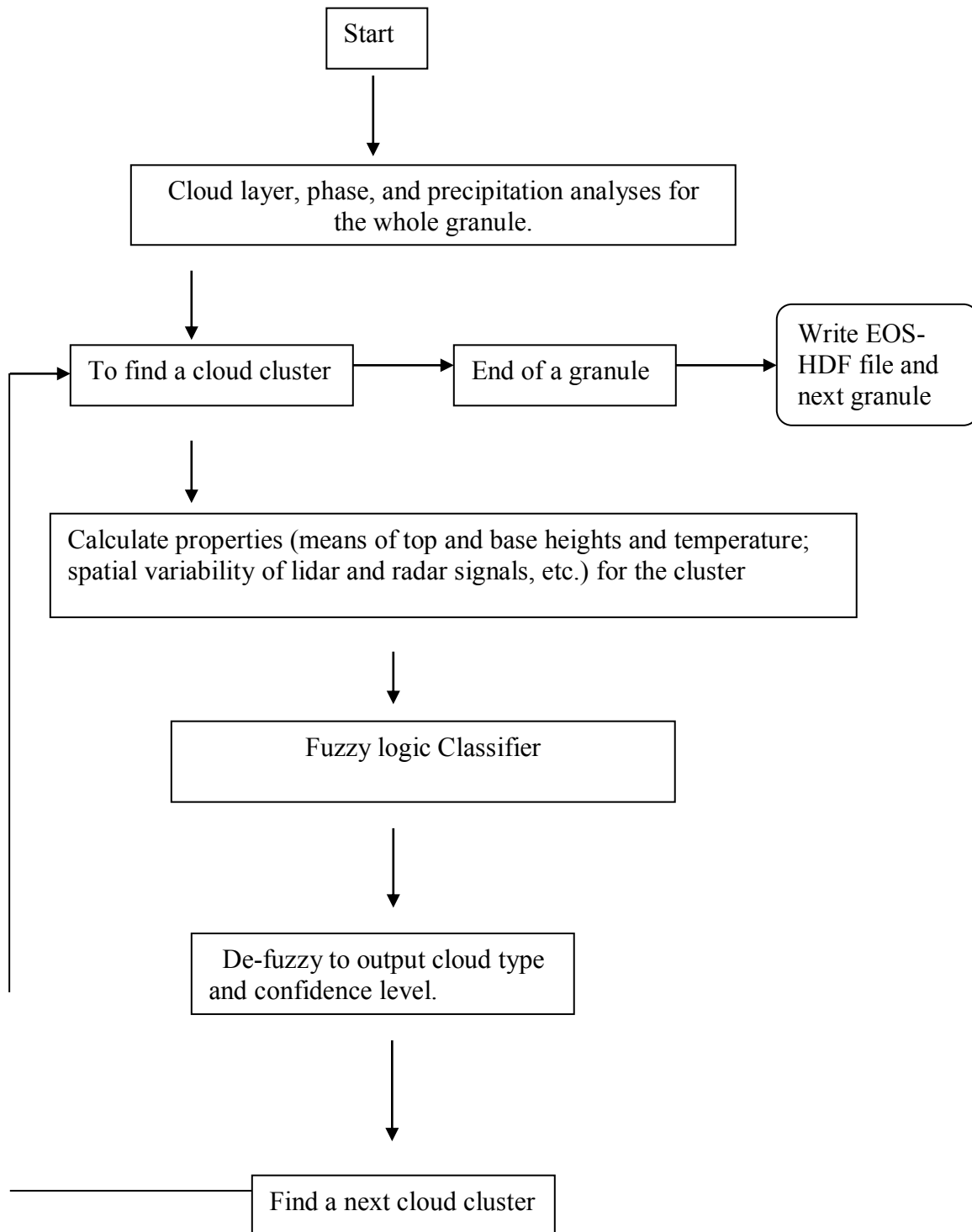
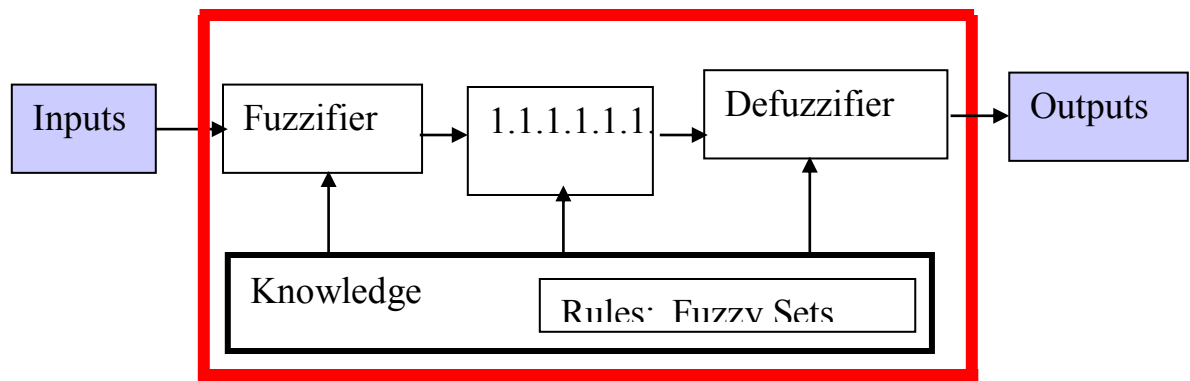


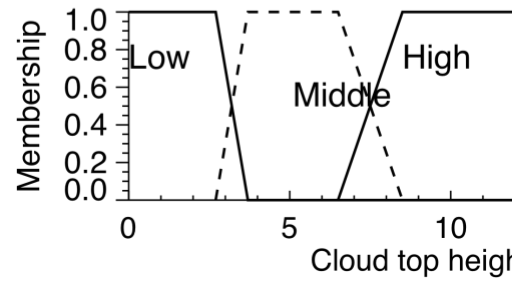
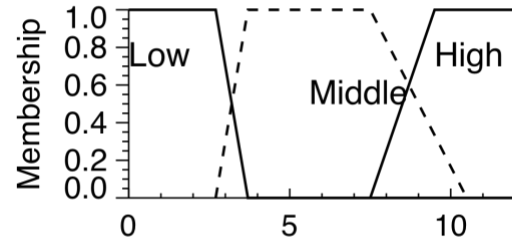
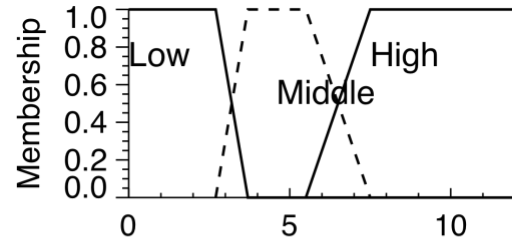
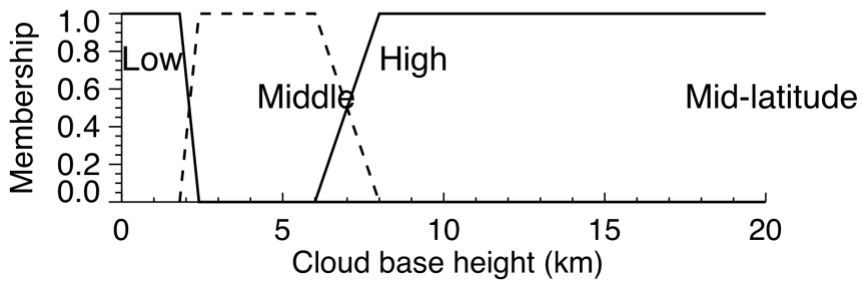
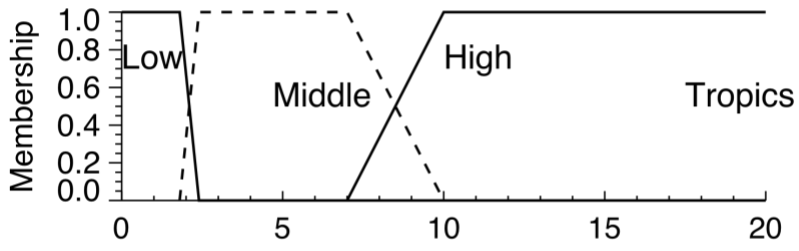
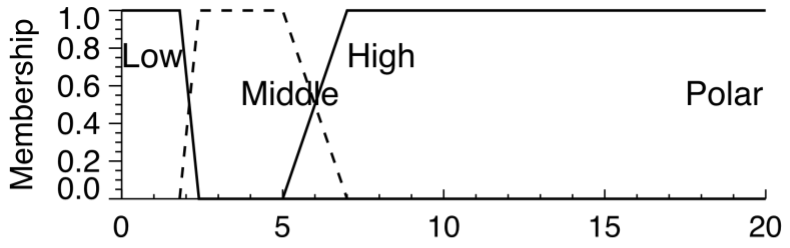
Figure 6: The algorithm flowchart for cloud scenario classification

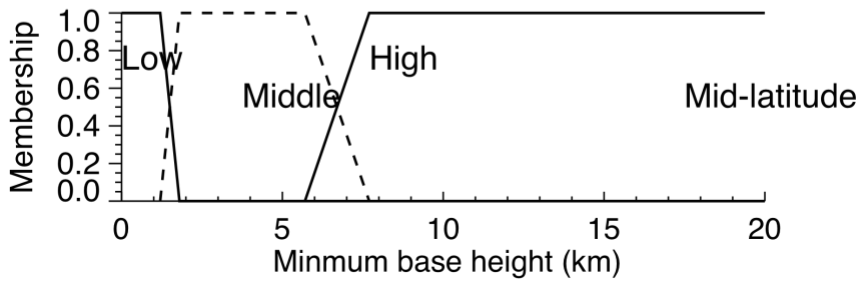
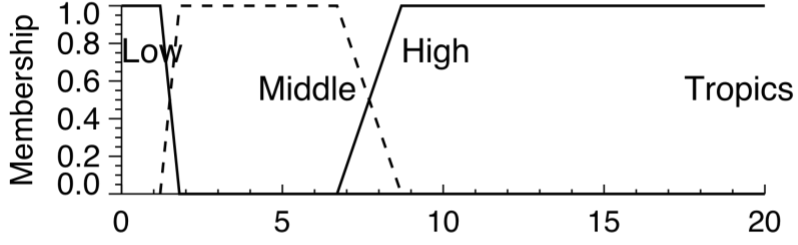
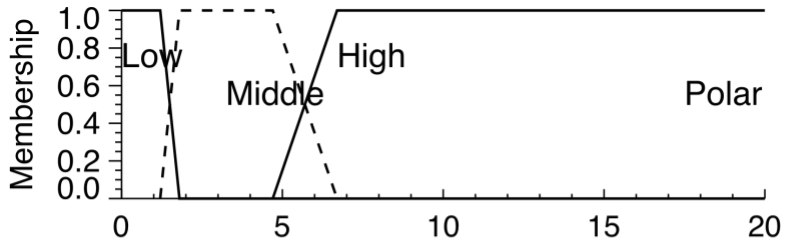
4.3 Classification Method

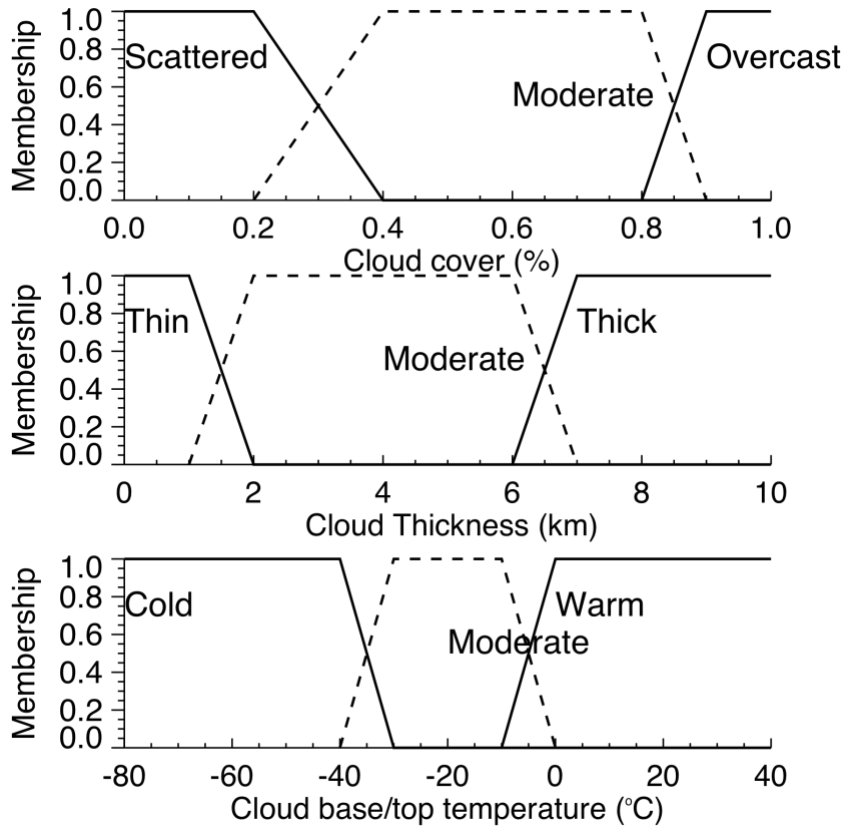
A combination of rule based and fuzzy logical based classification is used in this algorithm to improve classification flexibility. The cloud phase determination is based on rule-based logics and the cloud type classification is mainly based on the fuzzy logics. The general steps to use fuzzy logics for classification are schematically illustrated as:



A priori (expert) knowledge is needed to set the membership functions for the fuzzy sets. The membership functions of main fuzzy sets used in this algorithm are presented in Fig. 7. To calculate the membership of given fuzzy variable, the mean property of the cloud cluster is used. Currently, we use radar surface returns to simply measure precipitation intensity and only consider land and ocean differences.







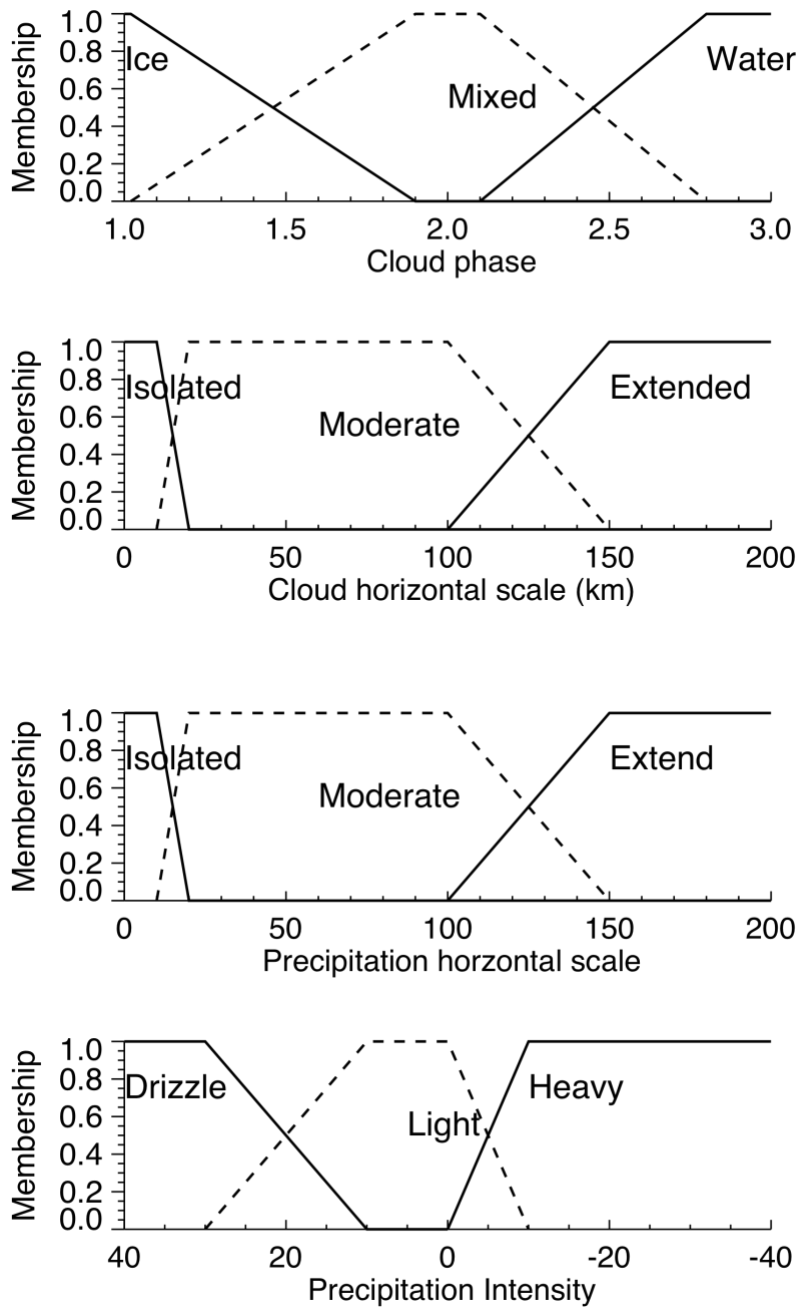


Figure 7: The membership functions for fuzzy variables of cloud top and base height and temperature, phase, cover, and thickness, and precipitation features.

Table 6 presents two examples to show how fuzzy logical based classification works. Based on the inputs, we will have different memberships (between 0 and 1) for different fuzzy sets. For example with $-53.0\text{ }^{\circ}\text{C}$ cloud base temperature, cold cloud base has a membership of 1 and moderate or warm cloud base has a membership of 0. The

membership for different cloud type can be between 0 and 1 too. For the first case, we have membership 1 for high cloud, and 0 for the others. Therefore, we are confident about the output. The second case is more complicated as there are two cloud types (high and As) with non-zero memberships. In the de-fuzzy process, we output a cloud type (high), which has the highest membership, and confidence level given by the normalized membership. However, there is option to output both cloud types with different confidence levels.

Table 6: Examples of fuzzy logical based classification

Inputs	Base_H	Top_H	dH	Base_T	Top_T	Cloud Fraction	Phase	
	8.52818	10.1073	1.57921	-53.0121	-63.0221	1.00000	3.00000	
Member- ships of fuzzy sets	Base temperature : cold, moderate, warm				1.00000	0.000000	0.000000	
	Cloud base height : Low, Mid, High				0.000000	0.000000	1.00000	
	Cloud thickness : Thin, Moderate, Thick				0.000000	1.00000	0.000000	
	Cloud cover : Scattered, Moderate, Overcast				0.000000	0.000000	1.00000	
Outputs	Cloud horizontal extend : Isolated, Moderate, Extended				0.000000	1.00000	0.000000	
	high_M,	As_M,	Ac_M,	St_M,	Sc_m,	Cu_M,	Ns_M,	Deep_M
	1.00000	0.000000	0.000000	0.000000	0.000000	0.000000	0.000000	0.000000

Base_H	Top_H	dH	Base_T	Top_T	Cloud Fraction	Phase	
7.47600	8.26350	0.787620	-38.8858	-43.7634	1.00000	3.00000	
Base temperature : cold, moderate, warm				0.888580	0.111420	0.000000	
Cloud base height : Low, Mid, High				0.000000	0.262000	0.738000	
Cloud thickness : Thin, Moderate, Thick				0.589114	0.410886	0.000000	
Cloud cover : Scattered, Moderate, Overcast				0.000000	0.000000	1.00000	
Cloud horizontal extend : Isolated, Moderate, Extended				0.000000	1.00000	0.000000	
high_M,	As_M,	Ac_M,	St_M,	Sc_m,	Cu_M,	Ns_M,	Deep_M
0.738000	0.262000	0.000000	0.000000	0.000000	0.000000	0.000000	0.000000

Notes:

Base_H, Base_T: cloud base height and temperature.

Top_H, Top_T: cloud top height and temperature.

dH: Cloud thickness.

High_M, As_M, Ac_M, St_M, Sc_M, Cu_M, Ns_M, and Deep_M: memberships for high, As, Ac, St, Sc, Cu, Ns, and Deep clouds.

To accommodate latitude dependent of tropopause height, we vary middle and high cloud definitions according to the latitude bands. The overlap between two variables (such as low cloud and middle cloud) provides the flexibility to hand errors in cloud base height and the freedom to use other parameters, such as cloud temperature (cold, moderate, and warm), precipitation intensity (drizzle, light, heavy), cloud thickness (thin, moderate, and thick), phase (ice, middle and water), to better define the outcomes with confidence

levels. As an example, the Table 7 lists the main fuzzy roles used to define As and Ac clouds.

Table 7: The fuzzy roles for As and Ac cloud classification

Property	As	Ac
Height and temperature (base and top)	Middle base; low base and middle or high top	Middle base; low base and middle top; warm or moderate cloud top temperature
Phase	Ice or mixed-phase	Mixed-phase or water
Precipitation	No precipitation or isolated drizzle	No precipitation or isolated or drizzle
Thickness	Moderate or thick or thin ice	Thin or moderate
Horizontal extend	Moderate or extend or mid-level ice	Isolated or moderated or extended mixed-phase
Cloud cover	Overcast or moderate mid-level ice clouds	Any

4.4 Precipitation Identification

Precipitation identification is an important step in the classification scheme. The current version algorithm, we use the same approach as the 2B-CLDCLASS product for the precipitation identification. But in the future version, we will use the precipitation flags in the CloudSat precipitation product.

4.5 Cloud Phase Identification

Although clouds can contain only water droplets when $> 0^{\circ}\text{C}$ and only ice crystals when $< -40^{\circ}\text{C}$, between 0 and -40°C , clouds can be of ice, water, or mixed phase composition (Rauber and Tokay 1991; Cober et al. 2001). Cloud properties associated with different cloud phases within this temperature range are complicated and not well known. To identify cloud phase, especially globally, is important to better understand cloud's role in climate change. Knowing cloud phase also allow for a better cloud type identification. For example, altostratus clouds are mainly ice clouds associated with synoptic scale motions. Due to small scale dynamics, local and embedded mixed-phase clouds can exist.

On the other hand, altocumulus clouds often exist as water or supercooled water with ice virga (mixed-phase). As documented by Zhang et al. (2010) mixed-phase altocumulus clouds are widely distributed.

CALIPSO level-2 scene identification provides water or ice cloud information based on the CALIOP measurements (Hu et al. 2009). However, there are few limitations to identify mixed-phase cloud correctly from space-based lidar measurements because of the strong impacts of multiple scatter on lidar depolarization measurements and the limited penetration of lidar for optically thick clouds. With coincident CloudSat and CALIPSO measurements, we developed a reliable approach to determine cloud layer phase (water, ice, and mixed-phase) and the location of water layer top to avoid the main limitations of the lidar-only based approach.

The approach is based on the fundamental microphysical and optical property differences between ice particle and water droplets. First, ice particles are much larger than water droplets. The large ice particles have terminal falling velocity about 1 m/s while small droplets have negligible falling velocity. This different vertical falling speeds affect cloud vertical distributions. Large particles are generally located near the bottom of ice clouds, while large water droplets are normally found near the top of water clouds. In the case of stratiform mixed-phase, ice particles grow quickly in the mixed-phase layer to form ice virga or precipitation below the mixed-phase layer. Second, there are orders of magnitude differences of cloud droplet and ice crystal number concentrations. Ice crystal number concentrations generally increase with temperature decrease and vary from less than $1/L$ to as high as $100/L$ within the temperature range warmer than homogeneous ice nucleation. Water droplet concentrations range from as low as $10/cm^3$ over clear marine boundary layer to as high as $500/cm^3$ over polluted continental boundary layer.

These microphysical property differences between water and ice phases result in large differences in their radiative properties, therefore, their different contributions to CALIPSO lidar and CloudSat signals (Wang and Sassen 2001). Due to weak attenuation of ice clouds, lidar signals can penetrate ice cloud layer up to a few kilometers. On the other hand, lidar signals are often attenuated by water clouds in just a few hundred meters. Although cloud droplet concentrations are much higher than ice crystal concentrations, CloudSat CPR Z_e in mixed-phase clouds are still dominated by ice particles because Z_e is proportional to the sixth power of particle size under the Rayleigh scattering region.

With these different sensitivities of CloudSat radar and CALIPSO lidar on ice crystals and water droplets, we can effectively determine the phase of a cloud layer. First, by locating a strong signal increase (slope and magnitude) followed by a strong signal

decrease due to attenuation, we detect the location of possible water layer (Wang and Sassen 2001). The cloud number concentration estimated from combined CloudSat and CALIPSO measurements are also used to improve water layer identification. Horizontally orientated plates do produce strong signals like a water layer, but it can be separated from a water layer by its weak attenuation after the strong signal increase.

With lidar identified water layer locations and the maximum radar signals in the layers, we can discriminate supercooled water layer with mixed-phase layer. A temperature dependent Z_e threshold was developed to detect ice occurrence (see Fig. 8, Zhang et al. 2010). If a cloud layer with top colder than -7°C and having supercooled water region and the layer maximum Z_e larger than the threshold, the cloud layer is regarded as a mixed-phase cloud layer. Otherwise, detected supercooled water layer is regarded as water phase.

The cloud top and base temperatures are also used as the first cut for the phase determination. Figure 9 shows the phase determine logics for lidar-radar detected cloud layers. The different logical paths for the phase determination contain different information, therefore different confidence levels. Together with the phase information for each cloud layer, we also output the confidence level as well as supercooled water layer top. **In the HDF file, the cloud phase has values from 1 to 3: 1-ice, 2-mixed-phase, and 3-water.**

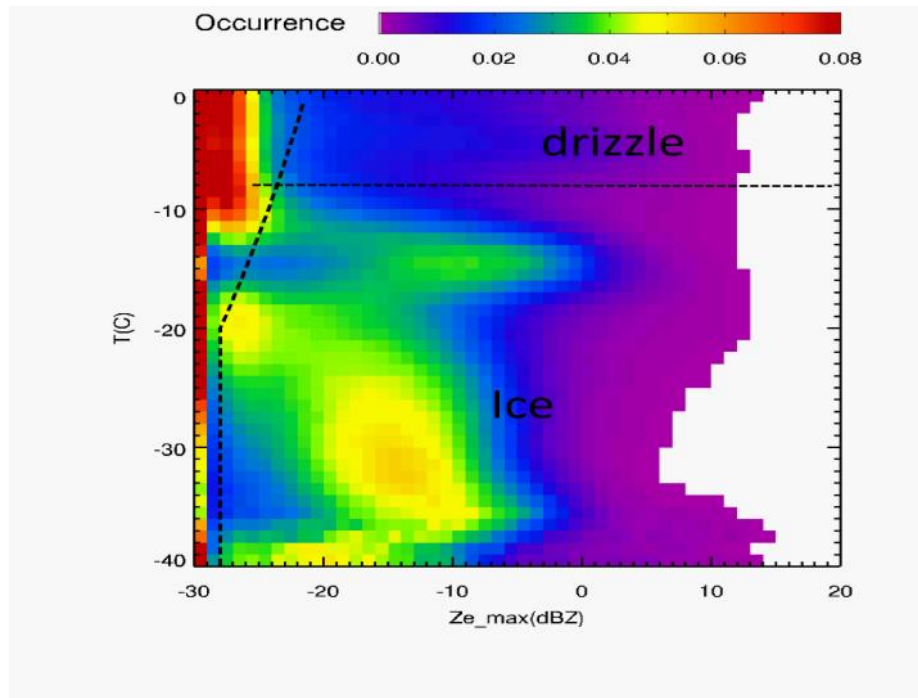


Figure 8. Water topped stratiform cloud distribution as a function of cloud top temperature and maximum Z_e within 500 m of the top. The thick dashed line indicate the Z_e thresholds.

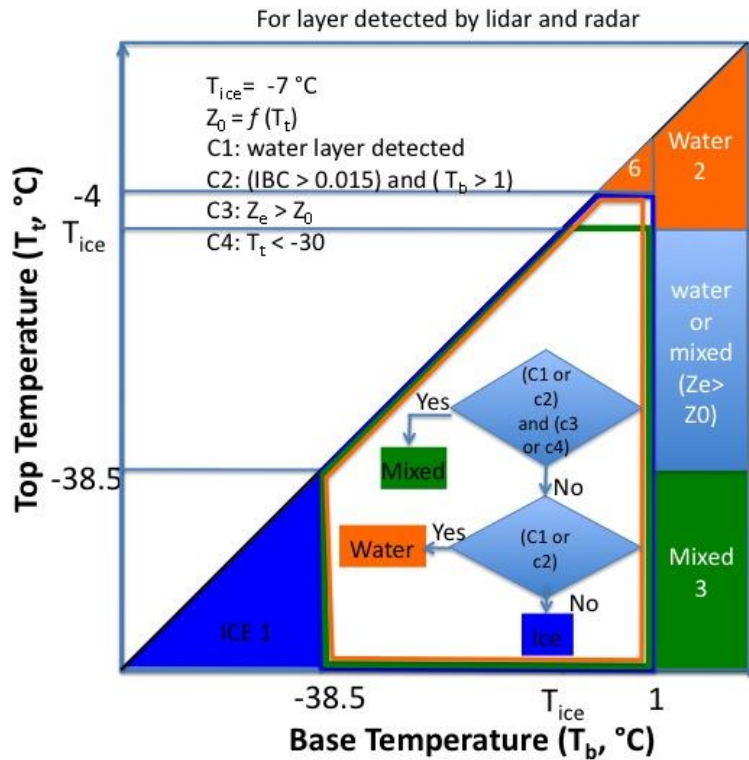


Figure 9. Logics for the phase determination of lidar-radar detected layers.

The approach didn't use lidar depolarization ratio and layer integrated attenuated backscattering coefficient (IBC) as CALIPSO phase determination (Hu et al. 2009), but perform well in terms of these layer lidar properties as illustrated in Fig.10. Horizontally oriented ice crystals, which are characterized by low depolarization and high IBC, are correctly identified as ice clouds or mixed-phase clouds. Due to the limited sensitivity of the CPR, it is very likely that report supercooled water layers may contain low concentration small ice crystals, but these ice particles should have a very small contribution on the total water content and optical depth of the cloud layer. Figure 11 show the seasonal cloud phase distribution map based on the 2007 and 2008 data.

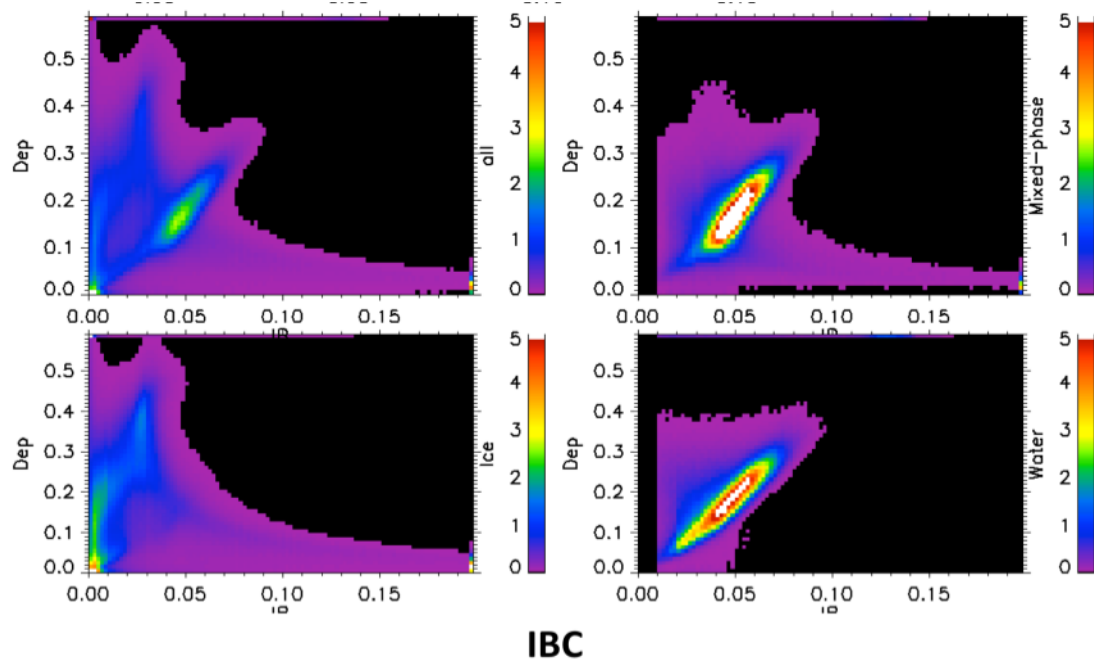


Figure 10. Cloud phase distribution in terms of layer mean depolarization ratio and integrated backscattering coefficient (IBC).

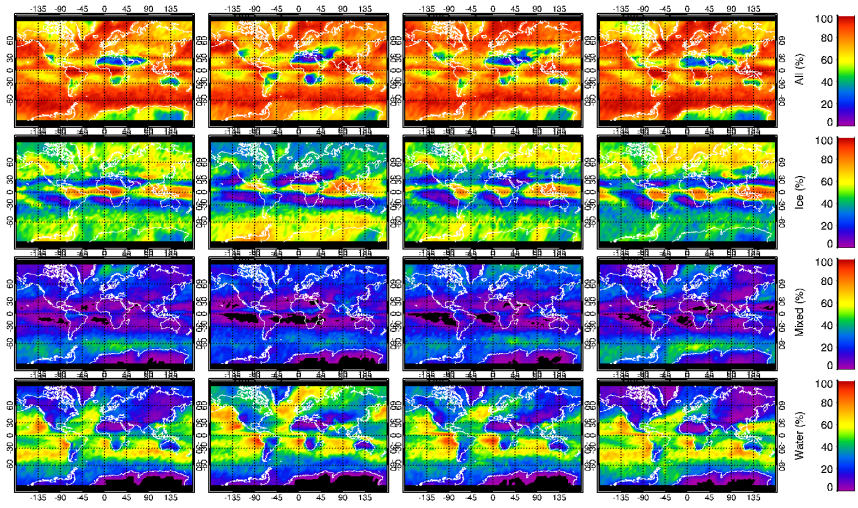


Figure 11. Seasonal cloud phase distributions based on 2007 and 2008 observations.

5 Data Product Output Format

The format consists of metadata, which describes the data characteristics, and swath data, which provide cloud type, phase and their qualities for each cloud layer. The different cloud types are outputted based on the following code:

-9 or 0 = Not determined

1 = High cloud

2 = Altostratus

3 = Altocumulus

4 = St

5 = Sc

6 = Cumulus

7 = Nimbostratus Cloud

8 = Deep Convection

The Appendix A provides more details for these outputs.

6 Operator Instructions

The Level 2 cloud scenario classification processing software will be integrated into CORE. It will be called using the standard CORE procedure for calling modules to operate on data files. The output will be in the form of an HDF-EOS structure in memory, which can be saved by CORE and passed on to other Level 2 processing.

This algorithm works at two different modes: radar only and combined radar and MODIS. If there are MODIS data and radar results indicate a single layer cloud system, algorithm selects the combined radar and MODIS mode, otherwise, algorithm uses radar only mode. But the combined radar and MODIS approach is still under development. The different modes are indicated in the outputs with algorithm flag.

For quality assessment purpose, statistics for cloud cover and height are generated. Average cloud covers within 300 CPR profiles are calculated for all clouds, high, middle (As and Ac), low (St, Sc and Cu) and thick (Ns and deep convective) clouds, respectively. The occurrence of multi-layer clouds can be seen from this statistics. The percentage of clouds masked by 2B-GEOPROF and analyzed in this algorithm is also given. It supposes to be 100%, and less than 100% means something wrong in the algorithm. The following is an example of output for cloud cover statistics form test data set 1.

***** Cloud Cover and Analysis Statistics *****

Index, Mean Lat, Mean Lon, Percentage of Cloud Mask Analyzed,
 Cloud Cover:All, High, Mid, Low,and Thick Clouds

1	1.475	93.484	100.000	59.000	18.667	34.333	29.333	0.000
2	4.422	92.859	100.000	39.667	12.333	14.000	41.000	0.000
3	7.369	92.230	100.000	24.000	9.333	17.000	0.000	0.000
4	10.316	91.596	100.000	49.333	7.667	45.667	0.333	0.000
5	13.261	90.954	100.000	65.667	20.000	43.667	3.333	24.667
6	16.205	90.301	100.000	2.000	2.000	0.333	0.000	0.000
7	19.148	89.634	100.000	18.333	4.333	15.333	0.000	0.000
8	22.088	88.951	100.000	75.000	5.667	66.000	6.000	22.000
9	25.025	88.248	100.000	18.000	2.667	14.667	5.333	0.000
10	27.960	87.520	100.000	55.000	61.333	0.667	0.000	0.000
11	30.891	86.763	100.000	99.333	44.667	3.000	5.000	96.000
12	33.818	85.972	100.000	89.667	35.333	32.333	2.667	43.000
13	36.740	85.139	100.000	84.667	10.333	79.667	0.000	0.000
14	39.657	84.257	100.000	8.000	6.333	0.667	2.667	0.000
15	42.568	83.315	100.000	2.333	2.667	0.333	0.000	0.000
16	45.473	82.301	100.000	79.667	37.333	45.333	0.000	0.000
17	48.368	81.200	100.000	49.000	11.333	49.333	0.000	0.000
18	51.255	79.991	100.000	31.333	9.667	32.333	0.667	0.000
19	54.130	78.648	100.000	3.667	4.000	0.000	0.000	0.000
20	56.990	77.136	100.000	21.667	1.667	4.667	1.667	16.000
21	59.834	75.407	100.000	40.667	42.667	0.000	0.000	0.000
22	62.711	73.348	100.000	95.333	24.667	28.000	7.333	52.333
23	65.529	70.922	100.000	85.667	8.667	5.667	53.333	34.333
24	68.279	67.993	100.000	76.667	6.333	11.333	42.000	30.333
25	70.970	64.325	100.000	19.000	2.667	5.333	0.000	11.333
26	73.576	59.581	100.000	36.333	4.000	33.667	2.333	0.000
27	76.048	53.225	100.000	32.667	36.333	0.000	0.000	0.000
28	78.302	44.419	100.000	36.000	20.333	28.000	0.667	0.000

Cloud height statistics (mean, standard deviation, maximum, and minimum of cloud base and top heights) for different type clouds in different latitudes are also calculated. These results provide useful information when algorithm or input data have problems. For example, if results indicate that high clouds occur below 2 km above sea level, there is something wrong in the algorithm or input data. An example of output for test data set one is given below. Cloud types 1 to 8 represent high, As, Ac, St, Sc, Cu, Ns, and deep convective clouds, respectively.

*****Cloud Height (base and top) Statistics for each type*****

Type	Mean	STD	Max	Min	
Whole Granuale Average					
1	11.038	6.007	28.797	5.037	Cloud base ←

1	12.381	5.560	28.917	5.157	Cloud top	←
2	4.205	1.719	12.477	-0.003		
2	6.360	2.658	14.997	0.597		
3	3.353	1.467	9.597	-0.003		
3	4.305	1.634	10.437	0.597		
4	0.176	0.364	2.157	-0.003		
4	0.867	0.519	2.757	0.117		
5	0.370	0.450	3.597	-0.003		
5	1.531	0.711	5.637	0.117		
6	1.032	1.213	6.957	-0.003		
6	2.187	1.621	11.397	0.117		
7	0.418	0.835	3.357	-0.003		
7	4.429	2.105	13.077	1.557		
8	1.169	1.408	3.837	-0.003		
8	5.423	1.898	12.837	1.557		
Tropical Average				-23.5 to 23.5	←	
1	13.059	5.730	28.797	5.037		
1	14.336	5.221	28.917	7.317		
2	4.887	1.829	9.837	0.717		
2	6.688	2.408	13.077	1.557		
3	3.786	1.949	9.597	-0.003		
3	5.390	2.171	10.437	2.757		
4	0.255	0.507	2.157	-0.003		
4	0.686	0.626	2.277	0.117		
5	0.507	0.539	2.637	-0.003		
5	1.467	0.813	4.917	0.117		
6	1.134	1.285	6.957	-0.003		
6	2.204	1.459	7.317	0.117		
7	0.420	0.737	3.357	-0.003		
7	4.325	1.394	9.477	1.557		
8	0.697	1.149	3.837	-0.003		
8	4.651	1.338	8.277	1.557		
Subtropical Average				-35 to -23.5 and 23.5 to 35	←	
1	11.247	5.631	28.797	5.037		
1	12.561	5.283	28.917	5.397		
2	4.048	1.262	9.837	0.717		
2	5.275	1.549	13.317	2.037		
3	3.629	2.104	6.477	0.957		
3	4.133	2.168	6.837	1.077		
4	0.053	0.258	1.437	-0.003		
4	0.559	0.439	2.037	0.117		
5	0.849	0.571	3.597	-0.003		
5	1.701	0.501	3.957	0.357		
6	1.235	1.429	5.517	-0.003		
6	1.918	1.476	5.877	0.117		
7	0.250	0.625	3.357	-0.003		
7	3.710	1.704	9.477	1.557		
8	2.224	1.766	3.837	-0.003		

8	5.790	1.090	8.277	2.757
Midlatitude Average -55 to -35 and 35 to 55				
1	11.213	6.676	28.797	5.037
1	12.375	6.204	28.917	5.157
2	4.218	1.245	12.477	1.437
2	6.483	2.394	14.757	2.277
3	3.338	0.737	5.277	0.237
3	4.158	0.633	5.877	2.757
4	0.077	0.274	1.437	-0.003
4	0.782	0.428	2.037	0.117
5	0.231	0.397	3.357	-0.003
5	1.539	0.750	5.637	0.117
6	0.824	1.124	6.477	-0.003
6	2.011	1.548	7.557	0.117
7	1.142	1.262	3.357	-0.003
7	6.052	2.771	10.437	1.557
8	1.651	1.359	3.837	-0.003
8	5.462	1.660	10.677	1.797
High latitude Average -90 to -55 and 55 to 90				
1	9.891	5.687	28.797	5.037
1	11.356	5.260	28.917	5.157
2	3.879	1.962	10.557	-0.003
2	6.529	3.157	14.997	0.597
3	2.877	1.193	5.037	0.237
3	3.581	1.136	6.357	0.597
4	0.216	0.282	2.157	-0.003
4	1.161	0.329	2.757	0.357
5	0.427	0.341	3.117	-0.003
5	1.527	0.597	4.917	0.117
6	0.999	1.093	5.517	-0.003
6	2.374	1.814	11.397	0.117
7	0.302	0.700	3.357	-0.003
7	4.438	2.066	13.077	1.557
8	0.808	1.227	3.837	-0.003
8	5.710	2.310	12.837	1.797

Another quick look for the performance of algorithm is to plot cloud type profile together with radar reflectivity and cloud mask profiles. An example of this plot is given in next page. Horizontal and vertical distributions of cloud types can be easily examined from this kind of plot.

7 References

- Ackerman, S. A., K. I. Strabala, W. P. Menzel, R. A. Frey, C. C. Moeller, and L. E. Gumley, 1998: Discriminating clear sky from clouds with MODIS. *J. Geophys. Res.*, **32**, 141-32,157.
- Bankert, R. L., 1994: Cloud classification of AVHRR imagery in maritime regions using a probabilistic neural network. *J. Appl. Meteor.*, **33**, 909-918.
- Chen, T., W. B. Rossow, and Y. Zhang, 2000: Cloud type radiative effects from the international satellite cloud climatology project. Proc. *11th Symposium on Global Change Studies*, Long Beach, California, American Meteorological Society, 86- 89.
- Cober, S. G., G. A. Isaac, A. V. Korolev, and J. W. Strapp, 2001: Assessing cloud phase condition conditions, *J. Appl. Meteor.*, **40**, 1967-1983.
- Deng, M. G. G. Mace, Z. Wang, and H. Okamoto, 2010: TC⁴ Validation for Ice Cloud Profiling Retrieval Using CloudSat Radar and CALIPSO Lidar, *J. Geophys. Res.*, **115**, D00J15, doi:10.1029/2009JD013104.
- Duchon, C. E., and M. S. O'Malley, 1999: Estimating cloud type from pyranometer observations. *J. Appl. Meteor.*, **38**, 132-141.
- Hartmann, D. L., M. E. Ockert-bell, and M. L. Michelsen, 1992: The effect of cloud type on Earth's energy balance: global analysis. *J. Climate*, **5**, 1281-1304.
- Hu, Y., D. Winker, M. Vaughan, B. Lin, A. Omar, C. Trepte, D. Flittner, P. Yang, S. L. Nasiri, B. Baum, W. Sun, Z. Liu, Z. Wang, S. Young, K. Stamnes, J. Huang, R. Kuehn, R. Holz 2009: CALIPSO/CALIOP Cloud Phase Discrimination Algorithm, *Journal of Atmospheric and Oceanic Technology*, **26**, 2293-2309.
- Luo, G., P. A. Davis, L. L. Stowe, and E. P. McClain, 1995: A pixel-scale algorithm of cloud type, layer, and amount for AVHRR data. Part I: nighttime. *J. Atmos. Oceanic Technol.*, **12**, 1013-1037.
- Moran, J. M., M. D. Morgan, and P. M. Pauley, 1997: *Meteorology: the Atmosphere and the Science of Weather*. Prentice-Hall, 530 pp.
- Parker, S. P., Editor in chief, 1988: *Meteorology Source Book*. McGraw-Hall, 304 pp.
- Penaloza, M. A., and R. M. Welch, 1996: Feature selection for classification of polar regions using a fuzzy expert system. *Remote Sens. Environ.*, **58**, 81-100.
- Rauber, R. M., and A. Tokay, 1991: An explanation for the existence of supercooled water at the tops of cold clouds. *J. Atmos. Sci.*, **48**, 1005-1023.
- Rossow, W. B., and R. A. Schiffer, 1999: Advances in understanding clouds from ISCCP. *Bull. Amer. Meteor. Soc.*, **80**, 2261-2286.
- Sassen K., 1991: The polarization lidar technique for cloud research: A review and current assessment. *Bull. Amer. Meteor. Soc.*, **72**, 1848-1866.

- Tovinkere, V. R., and M. Penaloza, A. Logar, J. Lee, R. C. Weger, T. A. Berendes, and R. M. Welch, 1993: An intercomparison of artificial intelligence approaches for polar scene identification. *J. Geophys. Res.*, **98**, 5001-5016.
- Uddstrom, M. J., and W. R. Gray, 1996: Satellite cloud classification and rain-rate estimation using multispectral radiances and measures of spatial texture. *J. Appl. Meteor.*, **35**, 839-858.
- Wang, Z. and K. Sassen, 2001: Cloud type and macrophysical property retrieval using multiple remote sensors. *J. Appl. Meteor.*, **40**, 1665-1682.
- Welch, R. M., S. K. Sengupta, A. K. Goroch, P. Rabindra, N. Rangaraj, and M. S. Navar, 1992: Polar cloud and surface classification using AVHRR imagery: An intercomparison of methods. *J. Appl. Meteor.*, **31**, 405-420.
- Williams, C. R., W. L. Ecklund, and K. S. Gage, 1995: Classification of precipitating clouds in the tropics using 915-MHz wind profilers. *J. Atmos. Oceanic Technol.*, **12**, 996-1012.
- World Meteorological Organization, 1956: *International Cloud Atlas: abridged atlas*. WMO, Geneva [c1969].
- Zhang, D., Z. Wang, and D. Liu, 2010: A Global View of Mid-level Liquid Layer Topped Stratiform Cloud Distributions and phase partition from CALIPSO and CloudSat Measurements, *J. Geophys. Res.*, *115*, D00H13, doi:10.1029/2009JD012143.
- Zhang, D., Z. Wang, T. Luo, Y. Yin, and C. Flynn, 2017: The occurrence of ice production in slightly supercooled Arctic stratiform clouds as observed by ground-based remote sensors at the ARM NSA site, *J. Geophys. Res. Atmos.*, *122*, doi:10.1002/2016JD026226.

8 Acronym List

Aqua	NASA's Earth Observing System PM Project
ARM	Atmospheric Radiation Measurement (ARM)
CIRA	Cooperative Institute for Research in the Atmosphere
CPR	Cloud Profiling Radar
CORE	CloudSat Operational and Research
EOS	Earth Observing System
HDF	Hierarchical Data Format
IFOV	Instantaneous field of view
IWC	Ice Water Content
LITE	Lidar In-space Technology Experiment
LWC	Liquid Water Content
MMCR	Millimeter- wave cloud radar
MODIS	Moderate Resolution Imaging Spectroradiometer
CALIPSO	Cloud-Aerosol Lidar and Infrared Pathfinder Satellite Observations
VTCW	Vehicle Time Code Word
SGP	The Southern Great Plains
NSA	The North Slope of Alaska
TWP	The Tropical Western Pacific
CART	Cloud and Radiation Testbed
CRYSTAL-FACE	The Cirrus Regional Study of Tropical Anvils and Cirrus Layers - Florida Area Cirrus Experiment
CPL	Cloud Physics Lidar
CRS	Cloud Radar System

9 Changes Since Algorithm Version P_R04

Above algorithm details are based on the R04 release. The major changes for the R05 are summarized below.

- a) The analysis of multi-year ground-based lidar and radar measurements of stratiform mixed-phase clouds indicated that ice particles are presented in these clouds when the cloud top temperature is colder than $-4\text{ }^{\circ}\text{C}$ (even for cases as warmer as -2°C) and radar detects significant echoes (Zhang et al. 2017). Based

on this study, the Tice threshold in the Fig.9 is changed from $-7\text{ }^{\circ}\text{C}$ to $-3\text{ }^{\circ}\text{C}$, which slightly increase mixed-phase cloud occurrence.

- b) Improved cloud clustering analysis: To avoid grouping low-level clouds with the middle- or high-level clouds, cloud clustering logics are improved to minimize the occurrence of these cases.
- c) The 2B-CLDCLASS-LIDAR uses the cloud fraction reported in the Lidar-aux, which is estimated with CALIOP measurements at the 330m horizontal resolution below the 8.2 km within the CPR footprint. The cloud fraction estimation algorithm was designed for warm boundary layer clouds, which underestimated cloud fractions for polar boundary layer ice clouds due to weaker signals. Now the 2B-CLDCLASS-LIDAR algorithm identifies the possible underestimation and avoids its impact on cloud type classification.
- d) Conditions are added to prevent classifying middle-level clouds with a mean top temperature colder than $-38\text{ }^{\circ}\text{C}$ as altocumulus (Ac).
- e) In the R04, some extensive shallow precipitating clouds were classified as the deep convective clouds, especially in the middle and high latitude. Now changes are made to classify them as Ns.

10 Open Issues and comments

Current outputs are limited to periods with both CPR and CALIOP observations. Thus, there are no cloud type outputs for the nighttime period during the DO-OP operation when only CALIOP measurements are available. In the future, it is possible to develop a lidar-only version of the classification.

Sc and St clouds are difficult to separate due to the footprint size of the averaged signals. Thus, it is better to combine them together as the boundary layer stratiform clouds for statistical analysis.

Cu clouds include fair weather cumulus and cumulus congestus. Fair weather cumulus is typically broken and geometrically thin clouds. Cumulus congestus are more vertically developed and often have top in the middle level. For statistical analyses, it is important to keep this in mind.

Polar regions present many difficult conditions for boundary layer cloud classification. For example, there are often optically ice clouds, which are difficult to fit into any traditional boundary layer cloud types.

Low and middle clouds are separated based on cloud base heights above the surface. Over mountain areas, we could have St, Sc, or Cu clouds with base heights above 7 km or higher in terms of the mean sea level. It is important to keep this in mind to better interpret statistical results.

11 Appendix A: 2B-CLDCLASS-LIDAR Interface Control Document

11.1 Input Field Specifications

(1) Seconds since the start of the granule

Name in file: Profile_time	Range: 0 to 6000
Source: 2B-GEOPROF 012	Missing value:
Field type (in file): REAL(4)	Missing value operator:
Field type (in algorithm): REAL(4)	Factor: 1
Dimensions: nray	Offset: 0
Units: seconds	MB: 0.139

Seconds since the start of the granule for each profile. The first profile is 0.

(2) Data status flags

Name in file: Data_status	Range: 0 to 127
Source: 2B-GEOPROF 012	Missing value:
Field type (in file): UINT(1)	Missing value operator:
Field type (in algorithm): UINT(1)	Factor: 1
Dimensions: nray	Offset: 0
Units: --	MB: 0.035

This is a bit field that contains data status flags:

- Bit 0: missing frame (0=false, 1=true)
- Bit 1: SOH missing (0=false, 1=true)
- Bit 2: GPS data valid (0=false, 1=true)
- Bit 3: 1 PPS lost (0=false, 1=true)
- Bit 4: Star tracker 1 (0=off, 1=on)
- Bit 5: Star tracker 2 (0=off, 1=on)
- Bit 6: Coast (0=false, 1=true)

Bit 7: NISC (0=false, 1=true)

(3) TAI time for the first profile

Name in file: TAI_start	Range: 0 to 6e+008
Source: 2B-GEOPROF 012	Missing value:
Field type (in file): REAL(8)	Missing value operator:
Field type (in algorithm): REAL(8)	Factor: 1
Dimensions: <scalar>	Offset: 0
Units: seconds	MB: 0

The TAI timestamp for the first profile in the data file. TAI is International Atomic Time: seconds since 00:00:00 Jan 1, 1993.

(4) Spacecraft Longitude

Name in file: Longitude	Range: -180 to 180
Source: 2B-GEOPROF 012	Missing value:
Field type (in file): REAL(4)	Missing value operator:
Field type (in algorithm): REAL(4)	Factor: 1
Dimensions: nray	Offset: 0
Units: degrees	MB: 0.139

Spacecraft geodetic longitude

(5) Spacecraft Latitude

Name in file: Latitude	Range: -90 to 90
Source: 2B-GEOPROF 012	Missing value:
Field type (in file): REAL(4)	Missing value operator:
Field type (in algorithm): REAL(4)	Factor: 1
Dimensions: nray	Offset: 0
Units: degrees	MB: 0.139

Spacecraft Geodetic Latitude.

(6) Range to the CPR boresight intercept with the geoid

Name in file: Range_to_intercept	Range: 600 to 800
Source: 2B-GEOPROF 012	Missing value:
Field type (in file): REAL(4)	Missing value operator:
Field type (in algorithm): REAL(4)	Factor: 1
Dimensions: nray	Offset: 0
Units: km	MB: 0.139

Range from the spacecraft to the CPR boresight intercept with the geoid.

(7) Height of range bin in Reflectivity/Cloud Mask above reference surface (~ mean sea level)

Name in file: Height	Range: -5000 to 30000
Source: 2B-GEOPROF 012	Missing value: -9999
Field type (in file): INT(2)	Missing value operator: ==
Field type (in algorithm): INT(2)	Factor: 1
Dimensions: nbin,nray	Offset: 0
Units: m	MB: 8.674

Height of the radar range bins in meters above mean sea level.

(8) Radar Reflectivity Factor

Name in file: Radar_Reflectivity	Range: -40 to 50
Source: 2B-GEOPROF 012	Missing value: -88.88
Field type (in file): INT(2)	Missing value operator: ==
Field type (in algorithm): REAL(4)	Factor: 0.01
Dimensions: nbin,nray	Offset: 0
Units: dBZe	MB: 8.674

Radar reflectivity factor Ze is calculated with the echo power and other input data as described in Li and Durden (2001)

(9) CPR Cloud Mask

Name in file: CPR_Cloud_mask	Range: 0 to 40
Source: 2B-GEOPROF 012	Missing value: -9
Field type (in file): INT(1)	Missing value operator: ==
Field type (in algorithm): INT(1)	Factor: 1
Dimensions: nbin,nray	Offset: 0
Units:	MB: 4.337

Each CPR resolution volume is assigned 1 bit mask value:

0 = No cloud detected

1 = likely bad data

5 = likely ground clutter

5-10 = weak detection found using along track integration.

20 to 40 = Cloud detected .. increasing values represents clouds with lower chance of a being a false detection.

(10) MODIS scene characterizations

Name in file: MODIS_scene_char	Range: 0 to 9
Source: 2B-GEOPROF 012	Missing value: -9
Field type (in file): INT(1)	Missing value operator: ==

Field type (in algorithm): INT(1) **Factor:** 1
Dimensions: nray **Offset:** 0
Units: **MB:** 0.035

This data includes MODIS pixel cloudiness characterization using cloudmask bit tests. See Table 3 for a detailed specification.

(11) MODIS scene variability

Name in file: MODIS_scene_var **Range:** 0 to 5
Source: 2B-GEOPROF 012 **Missing value:** -9
Field type (in file): INT(1) **Missing value operator:** ==
Field type (in algorithm): INT(1) **Factor:** 1
Dimensions: nray **Offset:** 0
Units: **MB:** 0.035

MODIS scene variability -variability of classification assigned to the 1 km MODIS pixels that compose the CloudSat footprint and immediately adjacent region. See Table 5 for a detail specification.

(12) Digital Elevation Map

Name in file: DEM_elevation **Range:** -9999 to 8850
Source: 2B-GEOPROF 012 **Missing value:** 9999
Field type (in file): INT(2) **Missing value operator:** ==
Field type (in algorithm): INT(2) **Factor:** 1
Dimensions: nray **Offset:** 0
Units: meters **MB:** 0.069

Elevation in meters above Mean Sea Level. A value of -9999 indicates ocean. A value of 9999 indicates an error in calculation of the elevation.

(13) Land Sea Flag

Name in file: Navigation_land_sea_flag **Range:** 1 to 3
Source: 2B-GEOPROF 012 **Missing value:**
Field type (in file): UINT(1) **Missing value operator:**
Field type (in algorithm): INT(1) **Factor:** 1
Dimensions: nray **Offset:** 0
Units: -- **MB:** 0.035

Flag indicating whether spacecraft is over land or sea:

1 = land
2 = ocean
3 = coast

(14) Vertical Binsize

Name in file: Vertical_binsize	Range: to
Source: 2B-GEOPROF 012	Missing value: -9999
Field type (in file): REAL(4)	Missing value operator: ==
Field type (in algorithm): REAL(4)	Factor: 1
Dimensions: <scalar>	Offset: 0
Units: m	MB: 0

Effective vertical height of the radar range bin.

(15) Clutter Reduction Flag

Name in file: Clutter_reduction_flag	Range: to
Source: 2B-GEOPROF 012	Missing value:
Field type (in file): INT(1)	Missing value operator:
Field type (in algorithm): INT(1)	Factor: 1
Dimensions: nray	Offset: 0
Units:	MB: 0.035

A value of 1 indicates that an estimate of surface clutter has been subtracted from the observed return power in bins 2 through 5 above the surface. A value of 0 indicate that NO clutter reduction has been applied.

(16) Location of Surface Bin as determined by 1B CPR algorithm. The value here is shifted (as Height)

Name in file: SurfaceHeightBin	Range: 1 to 125
Source: 2B-GEOPROF 012	Missing value: -1
Field type (in file): INT(1)	Missing value operator: ==
Field type (in algorithm): INT(1)	Factor: 1
Dimensions: nray	Offset: 0
Units:	MB: 0.035

Location of Surface Bin as determined by 1B CPR algorithm. The value here is shifted (as is the Height matrix) so bins in neighboring rays are about the same height.

(17) Cloud Fraction

Name in file: CloudFraction	Range: 0 to 100
Source: 2B-GEOPROF-LIDAR 004	Missing value: -9
Field type (in file): INT(1)	Missing value operator: ==
Field type (in algorithm): INT(1)	Factor: 1
Dimensions: nbin,nray	Offset: 0
Units:	MB: 4.337

The CloudFraction reports the fraction of lidar volumes in a radar resolution volume that contains hydrometeors. It is recorded per ray and per bin as a 1-byte integer variable. It is a percentage from 0 to 100.

(18) Quality of radar and lidar data

Name in file: UncertaintyCF	Range: 0 to 100
Source: 2B-GEOPROF-LIDAR 004	Missing value: -9
Field type (in file): INT(1)	Missing value operator: ==
Field type (in algorithm): INT(1)	Factor: 1
Dimensions: nbin,nray	Offset: 0
Units:	MB: 4.337

The UncertaintyCF is a description of the quality of radar and lidar data. It is recorded per ray and per bin as 1-byte integer.

- 0 means that neither radar data nor lidar data was found.
- 1 indicates that only radar data has been found.
- 2 indicates that only lidar data has been found.
- 3 indicates that both radar data and lidar data were found.

(19) Number of hydrometeor layers

Name in file: CloudLayers	Range: 0 to 5
Source: 2B-GEOPROF-LIDAR 004	Missing value: -9

Field type (in file): INT(1)	Missing value operator: ==
Field type (in algorithm): INT(1)	Factor: 1
Dimensions: nray	Offset: 0
Units:	MB: 0.035

CloudLayers is a description of the number of the observed hydrometeor layers in the vertical column of the radar footprint. It is recoded per ray as 1-byte integer. Its value is from 0 to 5. A maximum of 5 layers are recorded.

(20) Height of Layer Base

Name in file: LayerBase	Range: 0 to 25000
Source: 2B-GEOPROF-LIDAR 004	Missing value: -99
Field type (in file): INT(2)	Missing value operator: ==
Field type (in algorithm): REAL(4)	Factor: 1
Dimensions: ncloud,nray	Offset: 0
Units: m	MB: 0.347

LayerBase is a description of the height of the observed hydrometeor layer base. It is recoded per ray as 4-byte float. Its value is from 0 to 25000. The units are meters.

(21) Height of layer top

Name in file: LayerTop	Range: 0 to 25000
Source: 2B-GEOPROF-LIDAR 004	Missing value: -99
Field type (in file): INT(2)	Missing value operator: ==
Field type (in algorithm): REAL(4)	Factor: 1
Dimensions: ncloud,nray	Offset: 0
Units: m	MB: 0.347

LayerTop is a description of the height of the observed hydrometeor layer top. It is recoded per ray as 4-byte float. Its value is from 0 to 25000. The units are meters.

(22) Flag of layer base

Name in file: FlagBase	Range: 0 to 3
Source: 2B-GEOPROF-LIDAR 004	Missing value: -9
Field type (in file): INT(1)	Missing value operator: ==
Field type (in algorithm): INT(1)	Factor: 1
Dimensions: ncloud,nray	Offset: 0
Units:	MB: 0.173

FlagBase is the contribution flag for each layer base. It tells which instrument has been used to identify the base height. It is recorded per ray as 1-byte integer.

- 0 means that neither radar nor lidar finds a layer base.
- 1 indicates that only the radar has found the base.
- 2 indicates that only the lidar has found the base.
- 3 indicates that both radar and lidar have found the base.
- 9 corresponds to missing data.

(23) Flag of layer top

Name in file: FlagTop	Range: 0 to 3
Source: 2B-GEOPROF-LIDAR 004	Missing value: -9
Field type (in file): INT(1)	Missing value operator: ==
Field type (in algorithm): INT(1)	Factor: 1
Dimensions: ncloud,nray	Offset: 0
Units:	MB: 0.173

FlagTop is the contribution flag for each layer top. It tells which instrument is finding the top height. It is recorded per ray as 1-byte integer.

- 0 means that neither radar nor lidar find a top.
- 1 indicates that only the radar has found the top.
- 2 indicates that only the lidar has found the top.
- 3 indicates that both radar and lidar have found the top.
- 9 corresponds to missing data.

(24) Specific humidity

Name in file: Specific_humidity	Range: to
Source: ECMWF-AUX 008	Missing value: -999
Field type (in file): REAL(4)	Missing value operator: ==
Field type (in algorithm): REAL(4)	Factor: 1
Dimensions: nbin,nray	Offset: 0
Units: kg/kg	MB: 17.349

(25) Temperature

Name in file: Temperature	Range: to
Source: ECMWF-AUX 008	Missing value: -999
Field type (in file): REAL(4)	Missing value operator: ==

Field type (in algorithm): REAL(4) **Factor:** 1
Dimensions: nbin,nray **Offset:** 0
Units: K **MB:** 17.349

(26) Atmospheric pressure

Name in file: Pressure **Range:** to
Source: ECMWF-AUX 008 **Missing value:** -999
Field type (in file): REAL(4) **Missing value operator:** ==
Field type (in algorithm): REAL(4) **Factor:** 1
Dimensions: nbin,nray **Offset:** 0
Units: Pa **MB:** 17.349

(27) Attenuated Backscatter 1064

Name in file: TAB1064 **Range:** 0 to 0.4
Source: LIDAR-AUX 004 **Missing value:** -9999
Field type (in file): REAL(4) **Missing value operator:** ==
Field type (in algorithm): REAL(4) **Factor:** 1
Dimensions: lidar_11_583,nray **Offset:** 0
Units: km⁻¹ sr⁻¹ **MB:** 80.915

Attenuated Backscatter 1064 in a CloudSat footprint

(28) Perpendicular Attenuated Backscatter 532

Name in file: PAB532 **Range:** 0 to 0.2
Source: LIDAR-AUX 004 **Missing value:** -9999
Field type (in file): REAL(4) **Missing value operator:** ==
Field type (in algorithm): REAL(4) **Factor:** 1
Dimensions: lidar_11_583,nray **Offset:** 0
Units: km⁻¹ sr⁻¹ **MB:** 80.915

Perpendicular Attenuated Backscatter 532 in a CloudSat footprint

(29) Total Attenuated Backscatter 532

Name in file: TAB532 **Range:** 0 to 0.4
Source: LIDAR-AUX 004 **Missing value:** -9999
Field type (in file): REAL(4) **Missing value operator:** ==
Field type (in algorithm): REAL(4) **Factor:** 1
Dimensions: lidar_11_583,nray **Offset:** 0
Units: km⁻¹ sr⁻¹ **MB:** 80.915

Total Attenuated Backscatter 532 in a CloudSat footprint

(30) Lidar Cloud Mask

Name in file: Mask	Range: 0 to 1
Source: LIDAR-AUX 004	Missing value: -99
Field type (in file): INT(1)	Missing value operator: ==
Field type (in algorithm): INT(1)	Factor: 1
Dimensions: Lidar60m,nray	Offset: 0
Units:	MB: 11.936

Lidar cloud mask detected at CloudSat footprint and 60 m vertical resolution

(31) Lidar 60m bin height

Name in file: height_lidar60m	Range: -2 to 30
Source: LIDAR-AUX 004	Missing value:
Field type (in file): REAL(4)	Missing value operator:
Field type (in algorithm): REAL(4)	Factor: 1
Dimensions: Lidar60m	Offset: 0
Units:	MB: 0.001

Lidar 60m bin height used for the 60m cloud mask

(32) Day/night flag

Name in file: Day_night_flag	Range: 0 to 1
Source: LIDAR-AUX 004	Missing value:
Field type (in file): INT(1)	Missing value operator:
Field type (in algorithm): INT(1)	Factor: 1
Dimensions: nray	Offset: 0
Units:	MB: 0.035

Day_night_flag from CALIPSO file: 0 day and 1 night

(33) Cloud fraction

Name in file: Cloud_fraction	Range: 0 to 100
Source: LIDAR-AUX 004	Missing value: -99
Field type (in file): REAL(4)	Missing value operator: ==
Field type (in algorithm): REAL(4)	Factor: 1
Dimensions: Lidar60m,nray	Offset: 0
Units: %	MB: 47.744

Cloud fraction in CloudSat footprint calculated with CALIPSO 330 m data. Cloud fraction smaller than 100% is reported mainly for boundary layer clouds.

(34) Number of CALIPSO profile collocated within a CloudSat footprint

Name in file: Col_count	Range: 0 to 15
Source: LIDAR-AUX 004	Missing value: -99
Field type (in file): INT(2)	Missing value operator: ==
Field type (in algorithm): INT(2)	Factor: 1
Dimensions: nray	Offset: 0
Units:	MB: 0.069

Number of CALIPSO profile collocated within a CloudSat footprint. The collocation is based on the surface footprint lats and lons of CloudSat and CALIPSO. The distance between them smaller than 1.14 at latitude smaller than 60 degree, and it is increase slightly as latitude increase.

11.2 Product Field Specifications

(1) Seconds since the start of the granule

Name in file: Profile_time	Range: 0 to 6000
Source: 2B-GEOPROF 012	Missing value:
Field type (in file): REAL(4)	Missing value operator:
Field type (in algorithm): REAL(4)	Factor: 1
Dimensions: nray	Offset: 0
Units: seconds	MB: 0.139

Seconds since the start of the granule for each profile. The first profile is 0.

(2) UTC seconds since 00:00 Z of the first profile

Name in file: UTC_start	Range: 0 to 86400
Source: 2B-GEOPROF 012	Missing value:
Field type (in file): REAL(4)	Missing value operator:
Field type (in algorithm): REAL(4)	Factor: 1

Dimensions: <scalar> **Offset:** 0
Units: seconds **MB:** 0

The UTC seconds since 00:00 Z of the first profile in the data file.

(3) TAI time for the first profile

Name in file: TAI_start **Range:** 0 to 6e+008
Source: 2B-GEOPROF 012 **Missing value:**
Field type (in file): REAL(8) **Missing value operator:**
Field type (in algorithm): REAL(8) **Factor:** 1
Dimensions: <scalar> **Offset:** 0
Units: seconds **MB:** 0

The TAI timestamp for the first profile in the data file. TAI is International Atomic Time: seconds since 00:00:00 Jan 1 1993.

(4) Spacecraft Latitude

Name in file: Latitude **Range:** -90 to 90
Source: 2B-GEOPROF 012 **Missing value:**
Field type (in file): REAL(4) **Missing value operator:**
Field type (in algorithm): REAL(4) **Factor:** 1
Dimensions: nray **Offset:** 0
Units: degrees **MB:** 0.139

Spacecraft Geodetic Latitude

(5) Spacecraft Longitude

Name in file: Longitude **Range:** -180 to 180
Source: 2B-GEOPROF 012 **Missing value:**
Field type (in file): REAL(4) **Missing value operator:**
Field type (in algorithm): REAL(4) **Factor:** 1
Dimensions: nray **Offset:** 0
Units: degrees **MB:** 0.139

Spacecraft geodetic longitude

(6) Height of range bin in Reflectivity/Cloud Mask above reference surface (~ mean sea level)

Name in file: Height	Range: -5000 to 30000
Source: 2B-GEOPROF 012	Missing value: -9999
Field type (in file): INT(2)	Missing value operator: ==
Field type (in algorithm): INT(2)	Factor: 1
Dimensions: nbin,nray	Offset: 0
Units: m	MB: 8.674

Height of the radar range bins in meters above mean sea level.

(7) Range to the CPR boresight intercept with the geoid

Name in file: Range_to_intercept	Range: 600 to 800
Source: 2B-GEOPROF 012	Missing value:
Field type (in file): REAL(4)	Missing value operator:
Field type (in algorithm): REAL(4)	Factor: 1
Dimensions: nray	Offset: 0
Units: km	MB: 0.139

Range from the spacecraft to the CPR boresight intercept with the geoid.

(8) Digital Elevation Map

Name in file: DEM_elevation	Range: -9999 to 8850
Source: 2B-GEOPROF 012	Missing value: 9999
Field type (in file): INT(2)	Missing value operator: ==
Field type (in algorithm): INT(2)	Factor: 1
Dimensions: nray	Offset: 0
Units: meters	MB: 0.069

Elevation in meters above Mean Sea Level. A value of -9999 indicates ocean. A value of 9999 indicates an error in calculation of the elevation.

(9) Vertical Binsize

Name in file: Vertical_binsize	Range: to
Source: 2B-GEOPROF 012	Missing value: -9999
Field type (in file): REAL(4)	Missing value operator: ==
Field type (in algorithm): REAL(4)	Factor: 1
Dimensions: <scalar>	Offset: 0
Units: m	MB: 0

Effective vertical height of the radar range bin.

(10) Nominal satellite pitch angle offset from nadir

Name in file: Pitch_offset	Range: -90 to 90
Source: 2B-GEOPROF 012	Missing value:
Field type (in file): REAL(4)	Missing value operator:
Field type (in algorithm): REAL(4)	Factor: 1
Dimensions: <scalar>	Offset: 0
Units: degrees	MB: 0

The pitch angle offset from nadir during normal operations. Pitch up is positive (radar points along the flight track in the direction of motion), down is negative (radar points along the flight track opposite the direction of motion).

(11) Nominal satellite roll angle offset from nadir

Name in file: Roll_offset	Range: -90 to 90
Source: 2B-GEOPROF 012	Missing value:
Field type (in file): REAL(4)	Missing value operator:
Field type (in algorithm): REAL(4)	Factor: 1
Dimensions: <scalar>	Offset: 0
Units: degrees	MB: 0

The roll angle offset from nadir during normal operations. Positive roll results in the radar pointing to the right of the flight track. Negative roll to the left.

(12) Data Quality

Name in file: Data_quality	Range: 0 to 127
Source: 2B-GEOPROF 012	Missing value:
Field type (in file): UINT(1)	Missing value operator:
Field type (in algorithm): INT(2)	Factor: 1
Dimensions: nray	Offset: 0
Units: --	MB: 0.035

Flags indicating data quality. If 0, then data is of good quality. Otherwise, treat as a bit field with 8 flags:

- 0: RayStatus_validity not normal.
- 1: GPS data not valid.
- 2: Temperatures not valid.
- 3: Radar telemetry data quality is not normal.
- 4: Peak power is not normal.
- 5: CPR calibration maneuver.
- 6: Missing frame.
- 7: Not used.

(13) Data status flags

Name in file: Data_status	Range: 0 to 127
Source: 2B-GEOPROF 012	Missing value:
Field type (in file): UINT(1)	Missing value operator:
Field type (in algorithm): UINT(1)	Factor: 1
Dimensions: nray	Offset: 0
Units: --	MB: 0.035

This is a bit field that contains data status flags:

- Bit 0: missing frame (0=false, 1=true)
- Bit 1: SOH missing (0=false, 1=true)
- Bit 2: GPS data valid (0=false, 1=true)
- Bit 3: 1 PPS lost (0=false, 1=true)
- Bit 4: Star tracker 1 (0=off, 1=on)
- Bit 5: Star tracker 2 (0=off, 1=on)
- Bit 6: Coast (0=false, 1=true)
- Bit 7: NISC (0=false, 1=true)

(14) CPR bus orientation (target ID)

Name in file: Data_targetID	Range: 0 to 81
Source: 2B-GEOPROF 012	Missing value:
Field type (in file): UINT(1)	Missing value operator:
Field type (in algorithm): INT(1)	Factor: 1
Dimensions: nray	Offset: 0
Units: --	MB: 0.035

The target id indicates the orientation of the spacecraft bus. For normal operations the target ID is 0. The complete ID table is listed below:

Control Frame 0

0: CPR to point in 300 seconds - Nominal science mode
1 - 15: Target ID for testing - not planned for operational use

Control Frame 0, CPR Calibration

16: CPR to point in 160 seconds
17: CPR 15° to the right
18: CPR 15° to the left
19: CPR 10° to the right -- default rotation
20: CPR 10° to the left -- default rotation
21: CPR 5° to the right
21: CPR 5° to the left
23 - 29: Target ID for testing - not planned for operational use
30 - 36: CPR rotation - not planned for operational use
37 - 39: Not planned for operational use

Control Frame 1, Four thruster closed-loop

40: Rotation into the OR orientation
41: Rotation into the x-track along the anti-ang momentum
42: Rotation into the x-track along ang momentum
43: Rotation into the orbit lower orientation
44: Rotation into alt. OR w/ CPR away from Sun
45 - 49: Not planned for operational use

Control Frame 2, One thruster open-loop

50: Rotation into the OR orientation
51: Rotation into the x-track along the anti-ang momentum
52: Rotation into the x-track along ang momentum
53: Rotation into the orbit lower orientation
54: Rotation into alt. OR w/ CPR away from Sun
55 - 59: Not planned for operational use

Control Frame 3, Two thruster open-loop

60: Rotation into the OR orientation
61: Rotation into the x-track along the anti-ang momentum
62: Rotation into the x-track along ang momentum
63: Rotation into the orbit lower orientation
64: Rotation into alt. OR w/ CPR away from Sun
65 - 69: Not planned for operational use

Control Frame 4, Four thruster open-loop

- 70: Rotation into the OR orientation
- 71: Rotation into the x-track along the anti-ang momentum
- 72: Rotation into the x-track along ang momentum
- 73: Rotation into the orbit lower orientation
- 74: Rotation into alt. OR w/ CPR away from Sun
- 75 - 80: Not planned for operational use

Control Frame 5

81: Body into the x-track along the anti-ang momentum 82 - 1023: Not planned for operational use

(15) Cloud Layer

Name in file: Cloudlayer	Range: 0 to 10
Source: 2B-CLDCLASS-LIDAR 000	Missing value: -9
Field type (in file): INT(1)	Missing value operator: ==
Field type (in algorithm): INT(1)	Factor: 1
Dimensions: nray	Offset: 0
Units:	MB: 0.035

The total cloud layer by combining radar and lidar measurements

(16) Cloud Layer Base

Name in file: CloudLayerBase	Range: 0 to 20
Source: 2B-CLDCLASS-LIDAR 000	Missing value: -99
Field type (in file): REAL(4)	Missing value operator: ==
Field type (in algorithm): REAL(4)	Factor: 1
Dimensions: ncloud,nray	Offset: 0
Units: km	MB: 0.694

Combined cloud base height

(17) Layer Base Flag

Name in file: LayerBaseFlag	Range: to
Source: 2B-CLDCLASS-LIDAR 000	Missing value: -9
Field type (in file): INT(1)	Missing value operator: ==
Field type (in algorithm): INT(1)	Factor: 1
Dimensions: ncloud,nray	Offset: 0
Units:	MB: 0.173

For the base 1 for radar and 2 for lidar when both lidar and radar detected layer. When only lidar detected a cloud layer, such as supercooled water cloud, we assign 3 for it

(18) Cloud Layer Top

Name in file: CloudLayerTop	Range: 0 to 20
Source: 2B-CLDCLASS-LIDAR 000	Missing value: -99
Field type (in file): REAL(4)	Missing value operator: ==
Field type (in algorithm): REAL(4)	Factor: 1
Dimensions: ncloud,nray	Offset: 0
Units: km	MB: 0.694

Combined cloud top height

(19) Layer top Flag

Name in file: LayerTopFlag	Range: 1 to 3
Source: 2B-CLDCLASS-LIDAR 000	Missing value: -9
Field type (in file): INT(1)	Missing value operator: ==
Field type (in algorithm): INT(1)	Factor: 1
Dimensions: ncloud,nray	Offset: 0
Units:	MB: 0.173

For the top 1 for radar and 2 for lidar when both lidar and radar detected layer. When only lidar detected a cloud layer, such as supercooled water cloud, we assign 3 for it

(20) Cloud Fraction

Name in file: CloudFraction	Range: 0 to 1
Source: 2B-CLDCLASS-LIDAR 000	Missing value: -99
Field type (in file): REAL(4)	Missing value operator: ==
Field type (in algorithm): REAL(4)	Factor: 1
Dimensions: ncloud,nray	Offset: 0
Units:	MB: 0.694

Cloud fraction within CloudSat foot print determined from CALIPSO lidar measurements.

(21) Cloud Phase

Name in file: CloudPhase	Range: 1 to 3
Source: 2B-CLDCLASS-LIDAR 000	Missing value: -9
Field type (in file): INT(1)	Missing value operator: ==
Field type (in algorithm): INT(1)	Factor: 1
Dimensions: ncloud,nray	Offset: 0
Units:	MB: 0.173

Cloud phase identified by using CALIPSO feature, temperature, and radar reflectivity
1-ice, 2 mixed, 3-water

(22) Cloud Phase Confidence Level

Name in file: CloudPhaseConfidenceLevel	Range: 0 to 10
Source: 2B-CLDCLASS-LIDAR 000	Missing value: -9
Field type (in file): INT(1)	Missing value operator: ==
Field type (in algorithm): INT(1)	Factor: 1
Dimensions: ncloud,nray	Offset: 0
Units:	MB: 0.173

Confidence level assigned to the cloud phase for each layer. It has a value ranging from 0 to 10. 10 indicates the highest confidence level. If confidence level is below 5, use the cloud phase with a caution.

(23) Cloud Layer Type

Name in file: CloudLayerType	Range: 0 to 8
Source: 2B-CLDCLASS-LIDAR 000	Missing value: -9
Field type (in file): INT(1)	Missing value operator: ==
Field type (in algorithm): INT(1)	Factor: 1
Dimensions: ncloud,nray	Offset: 0
Units:	MB: 0.173

Cloud type for each layer.

- 0 = Not determined
- 1 = Cirrus
- 2 = Altostratus
- 3 = Altocumulus
- 4 = Stratus
- 5 = Stratocumulus
- 6 = Cumulus
- 7 = Nimbostratus
- 8 = Deep convection

(24) Cloud Type Quality

Name in file: CloudTypeQuality **Range:** 0 to 1
Source: 2B-CLDCLASS-LIDAR 000 **Missing value:** -99
Field type (in file): REAL(4) **Missing value operator:** ==
Field type (in algorithm): REAL(4) **Factor:** 1
Dimensions: ncloud,nray **Offset:** 0
Units: **MB:** 0.694

Cloud Type Quality decided based on fuzzy-logic classification.

(25) Precipitation Flag

Name in file: PrecipitationFlag **Range:** -1 to 3
Source: 2B-CLDCLASS-LIDAR 000 **Missing value:** -9
Field type (in file): INT(1) **Missing value operator:** ==
Field type (in algorithm): INT(1) **Factor:** 1
Dimensions: ncloud,nray **Offset:** 0
Units: **MB:** 0.173

Precipitation flag indicate whether the cloud layer produces precipitation.

Precipitation flag has the following values:

- 1 = not determined
- 0 = no precipitation
- 1 = liquid precipitation
- 2 = solid precipitation
- 3 = possible drizzle (?)

(26) The logical path of phase determination

Name in file: Phase_log **Range:** 0 to 3
Source: 2B-CLDCLASS-LIDAR 000 **Missing value:** -9
Field type (in file): INT(1) **Missing value operator:** ==
Field type (in algorithm): INT(1) **Factor:** 1
Dimensions: ncloud,nray **Offset:** 0
Units: **MB:** 0.173

Record the logical path of phase determination

(27) Water layer top

Name in file: Water_layer_top **Range:** -9 to 12
Source: 2B-CLDCLASS-LIDAR 000 **Missing value:** -9
Field type (in file): REAL(4) **Missing value operator:** ==
Field type (in algorithm): REAL(4) **Factor:** 1

Dimensions: ncloud,nray
Units: km

Offset: 0
MB: 0.694

This provides water layer top height in mixed-phase and water clouds. This is mainly to indicate the location of possible water layer in mixed-phase clouds.